修士論文

A search for neutrinoless tau decays $\tau \to e/\mu\ K^0$ at Belle experiment.

(Belle実験におけるニュートリノレス $\tau \to e/\mu\ K^0$ 崩壊の探索)

東北大学大学院理学研究科

物理学専攻

遊佐 洋右

平成１３年

Acknowledgments

Abstract

The observation of lepton flavor violation (LFV) would be evidence of new physics beyond the Standard Model. We might expect that a non-zero neutrino mass, as inferred from neutrino oscillations at Super Kamiokande [1], could give rise to lepton flavor violating neutrinoless τ decays, such as: $\tau \rightarrow \mu\gamma$, $\tau \rightarrow \ell$ + two charged particles and $\tau \rightarrow \ell\, M^0$, where $\ell = (e/\mu)$ and $M^0 = \pi^0$, ρ^0, ϕ, K^{*0}, K^0, etc. In models with heavy neutral leptons, some of these branching ratios are predicted to be of the order of 10^{-6} [2, 3].

As a B-factory, KEKB [4] produces as many τ pair events as $B\bar{B}$ events, the τ LFV process could be searched with high statistics at Belle experiment. In this thesis, we report a search for $\tau \rightarrow \ell\, K^0$ decays from 30 fb^{-1} of asymmetric, 3.5 GeV $\times$ 8.0 GeV, e^+e^- collisions data at KEKB. The total energy of an e^+e^- collision, in the center of mass (CM) system, is 10.58 GeV, the energy of the $\Upsilon(4S)$ resonance. We observe no $\tau \rightarrow \ell$ candidates, and set upper limits of branching ratios to be $Br(\tau \rightarrow e\, K^0) < 0.94 \times 10^{-6}$ and $Br(\tau \rightarrow \mu\, K^0) < 0.94 \times 10^{-6}$ 90% C.L.. This is an improvement more than factor of 10^{-3} than the results of MARKII using 17 pb^{-1} of data which set the upper limit on the branching ratio of $\tau \rightarrow \ell K^0$ decays [5] and almost same amplitude as the other upper limits on the branching ratios for these decay modes, except for $\tau \rightarrow \ell\, K^0$ that were obtained by the CLEO II experiment. [6].

Contents

5   Conclusions   50

A   Other lepton flavor violating τ decay modes   52

Bibliography   62

List of Figures

List of Tables

Chapter 1

Introduction

The significant result from B-factories has been appeared last summer [7, 8]. We have got a firm evidence of CP-violation in B^0 meson decays. The Cabbibo-Kobayashi-Masukawa matrix contains information of mixing of quarks in the process of weak interaction. On the other hand, lepton part of GIM mechanism has no equivalence to Cabbibo angle because the Standard Model was constructed under the assumption of the zero-mass neutrinos. Thus, lepton flavor is conserved. But in these days, we might expect that a non-zero neutrino mass as inferred from neutrino oscillations at Super Kamiokande [1] could give rise to violate lepton flavor conservation in lepton decay. If we observe lepton flavor violating process, it would be evidence of new physics beyond the Standard Model. Lepton flavor violation has been searched by many experiments so far, but no lepton flavor violating process was observed. Generally, the searches are classified as to search for the lepton flavor violating process from muon decay or τ decay. To obtain the τ sample is harder than muon sample, but the branching ratios of τ lepton flavor violating processes predicted from theories are much larger than that of muons because τ is about 17 times heavier than muon. To generate τ pair in e^+e^- collision, we need the accelerator of the center-of-mass energy of more than $2m_\tau$ (m_τ is the mass of τ). KEKB accelerator satisfies that with high luminosity. We can study not only B-physics but also τ-physics at BELLE experiment. The CLEO II that also aim for B-physics with e^+e^- collider, has searched for lepton flavor violating process from τ and set upper limits on the branching ratios of all modes of the type $\tau \to 3$ charged except for $\tau \to \ell \ K^0$ (ℓ stands for electron or muon.). They set the upper limits the order of 10^{-6} to 10^{-5} at 90% C.L. from the analysis of an integrated luminocity of 4.79 fb^{-1} of the data. Upper limits for the branching ratio of $\tau \to \ell \ K^0$ have been measured to be 1.3×10^{-3} for $\tau \to e \ K^0$, and 1.0×10^{-3} for $\tau \to \mu \ K^0$ at 90 % C.L., using data recorded by MARK II from 17 pb^{-1} of integrated luminocity at SPEAR. In this thesis, we report the results of searching for lepton flavor violating process of $\tau \to \ell \ K_S$. We use an integrated luminocity of 30 fb-1 of the data delivered by KEKB and recorded by Belle detector. In the following chapters, physics and formalism about lepton flavor and its violation is first given in Chapter 2 and an introduction to a B-factory experiment at KEK is given in Chapter 3. We then move to analysis. The event selection and result of analysis isdescribed in Chapter

4. Finally, we conclude Chapter 5.

Chapter 2

Physics

This chapter covers the physics and formalism of $\tau \to \ell\, M^0$ modes, where $\ell = (e/\mu)$ and $M^0 = \pi^0$, ρ^0, ϕ, K^{*0}, K^0, etc.. These modes will appear if we extend the Standard Model with suprrsymmetry (SUSY). First, we mention why the lepton flavor violating modes are forbided in the Standard Model, and then describe about the candidates which enhance the appearance of lepton flavor violation.

2.1   Lepton flavor conservation in the Standard Model

Weinberg and Salam model which is based on the $SU(2)_L \times U(1)_Y$ gauge theory with spontaneous symmetry breaking has successful explained experimental results. The "Standard Model" is consist of this model and the quantum chromodynamics that describe the strong interaction by $SU(3)$ gauge theory. We describe quarks and leptons of k-th generation as follows:

$$q_{kL} = \begin{pmatrix} u_{kL} \\ d_{kL} \end{pmatrix}, u_{kR}, d_{kR}, l_{kL} = \begin{pmatrix} \nu_{kL} \\ e_{kL} \end{pmatrix}, e_{kR} \tag{2.1}$$

where

$$e_{kL} \equiv \frac{1 - \gamma_5}{2} e_k, \nu_{kL} \equiv \frac{1 - \gamma_5}{2} \nu_k,$$
$$u_{kL} \equiv \frac{1 - \gamma_5}{2} u_k, d_{kL} \equiv \frac{1 - \gamma_5}{2} d_k \tag{2.2}$$

because the helicitiy of antineutrinos which comes through the β decays is always +1 and that of electrons is -1 with an approximation of ignoring the mass. Also the $SU(2)$ doublet is introduced as Higgs scholar:

$$\phi = \begin{pmatrix} \phi^0 \\ \phi^- \end{pmatrix}. \tag{2.3}$$

We are able to describe the Lagrangian of coupling between W bosons and quarks/leptons as

$$\mathcal{L}_W = \frac{g}{\sqrt{2}}(\overline{\nu^0_{kL}}\gamma^\mu e^0_{kL}W^+_\mu + \overline{u^0_{kL}}\gamma^\mu d^0_{kL}W^+_\mu + h.c.) \tag{2.4}$$

where the Einstein's description; Lagrangian is summed up about the repeating suffix. The suffix 0 indicates that the quarks and leptons here is taken as the eigenstate of the interaction with W; not an eigenstate of the mass.

Quarks and leptons have the mass through Yukawa interaction with Higgs field after the symmetry breaking .

$$\mathcal{L}_{Yukawa} = y^{mn}_E \overline{l^0_{mL}}e^0_{nR}\tilde{\phi} + y^{mn}_D \overline{q^0_{mL}}d^0_{nR}\tilde{\phi} + y^{mn}_U \overline{q^0_{mL}}u^0_{nR}\phi + h.c. \tag{2.5}$$
$$= y^{mn}_E[(\phi^-)^*\overline{\nu^0_{mL}}e^0_{nR} - (\phi^0)^*\overline{e^0_{mL}}e^0_{nR}] +$$
$$y^{mn}_D[(\phi^-)^*\overline{u^0_{mL}}d^0_{nR} - (\phi^0)^*\overline{d^0_{mL}}d^0_{nR}] +$$
$$y^{mn}_U[(\phi^0)^*\overline{u^0_{mL}}u^0_{nR} + (\phi^-)^*\overline{d^0_{mL}}u^0_{nR}] + h.c. \tag{2.6}$$

This is the general description of Yukawa interaction because the relativistic invariance and gauge invariance do not forbid the coupling of the fields of different generations each other. Introducing the vacuum expectation $v\sqrt{2}$ into ϕ^0, we obtain the mass matrices of quarks and leptons:

$$(M_E)_{mn} = vy^{mn}_E/\sqrt{2}, \ (M_D)_{mn} = vy^{mn}_D/\sqrt{2}, \ (M_U)_{mn} = vy^{mn}_U/\sqrt{2}. \tag{2.7}$$

If we define the number of generations is n_F, any of these are the imaginary $n_F \times n_F$ matrix. We obtain the mass of quarks/leptons by diagonalizing through mutual unitary transformation:

$$U_{LX}M_X(U_{RX})^\dagger = \begin{pmatrix} m_{X_1} & & \\ & \ddots & \\ & & m_{X_{n_F}} \end{pmatrix}. \tag{2.8}$$

The mass eigenstate of quarks/leptons couples with the eigenstate of interaction by the unitary transformation which comes up here and describe as:

$$e_{Rm} = (U_{RE})_{mn}e^0_{Rn}, e_{Lm} = (U_{LE})_{mn}e^0_{Ln}, \tag{2.9}$$
$$d_{Rm} = (U_{RD})_{mn}d^0_{Rn}, d_{Lm} = (U_{LD})_{mn}d^0_{Ln}, \tag{2.10}$$
$$u_{Rm} = (U_{RU})_{mn}u^0_{Rn}, u_{Lm} = (U_{LU})_{mn}u^0_{Ln}. \tag{2.11}$$

Introducing this into (2.4),

$$\mathcal{L}_W = \frac{g}{\sqrt{2}}(\overline{\nu_{kL}^0}\gamma^\mu(U_{LE}^\dagger)_{kn}e_{nL}W_\mu^+ + \overline{u_{kL}}\gamma^\mu(U_{LU}U_{LD}^\dagger)_{kn}d_{nL}W_\mu^+ + h.c.). \qquad (2.12)$$

In the Standard Model, we assume the neutrino is degenerating with zero-mass. There is no effect to the physics in the process of the unitary transformation between each generations for neutrino. We set

$$\nu_{Lm} = (U_{LE})_{mn}\nu_{Ln}^0 \qquad (2.13)$$
$$U_{LU}U_{LD}^\dagger \equiv V_{KM} \qquad (2.14)$$

and thus obtain the Lagrangian for interaction as written below.

$$\mathcal{L}_W = \frac{g}{\sqrt{2}}(\overline{\nu_{kL}}\gamma^\mu e_{kL}W_\mu^+ + \overline{u_{kL}}\gamma^\mu(V_{KM})_{kn}d_{nL}W_\mu^+ + h.c.). \qquad (2.15)$$

This shows the quantum number of generation is conserved for leptons, but not conserved for quarks generally, as far as the V_{KM} is diagonalized.

2.2 Lepton flavor violation in extensions of the Standard Model

There are many extensions of the Standard Model as almost every of extension leads to lepton flavor/number violation (LFV/LNV). In this section, we focus two extended Standard Model. One is the Standard Model extended by heavy neutral leptons (model A)[9]. The other is extended by the minimal $SU(2)_L \times SU(2)_R \times U(1)_{B-L}$, manifestly left-right symmetric model (Model B) [10].

In the model A, the lepton content changes in (2,1):

$$l_{kL} = \begin{pmatrix} K_L^{\dagger\nu}\nu_{kL} + K_L^{\dagger N}N_{kL} \\ e_{kL} \end{pmatrix}, \; N_{kR}, \; e_{kR} \qquad (2.16)$$

where ν_{kL} are massless neutrinos, and N_k are heavy massive Dirac neutrinos. K_L is a CKM-type 6×3 matrix that is equivalent with V_{KM} in quark mixing. The notation $n_{kL} = (\nu_{kL}, N_{kL})$ is introduced. This model contains two LFV interactions: lnW and nnZ. LFV can be defined through charge-current Lagrangian,

$$\mathcal{L}_W^l = \frac{g}{\sqrt{2}}(\overline{e_{kL}}\gamma^\mu K_{kL}^\dagger n_{kL} W_\mu^- + h.c.). \tag{2.17}$$

In the model B, new fields and Standard Model fields with charged group structure are

$$Z_2, W_R^\pm; \begin{pmatrix} u_{kR} \\ (V_{KM})_R d_{kR} \end{pmatrix}; \overbrace{e_{kL}, n}^{2_L}, \overbrace{n, e_{kR}}^{2_R};$$
$$H_1^0, H_2^0, H_3^0, A_1^0, A_2^0, H_1^\pm, H_2^\pm, \delta_L^{\pm\pm}, \delta_R^{\pm\pm}. \tag{2.18}$$

Z_2 and $W_R^\pm$ are three additional very heavy gauge bosons that couple (predominantly) to the right-handed fields; right-handed quarks from $SU(2)_R$ doublet ($(V_{KM})_R$ is CKM matrix for the right-handed quarks); the lepton form left- and right-handed weak doublets, but the neutrinos from both doublets mix forming six physical fields n; $H_1^0, H_2^0, H_3^0, A_1^0, A_2^0, H_1^\pm, H_2^\pm, \delta_L^{\pm\pm}$ and $\delta_R^{\pm\pm}$ are additional very heavy Higgs bosons. Thus, there are eight additional interactions in addition to those in the model A: $l^\pm n H_{1,2}^\mp, l^\pm n G_{1,2}^\mp; ll H_{0,1,2}^0, ll A_1^0; ll \delta_{L,R}^{\pm\pm}; nn H_{0,1,2,3}^0, nn A_{1,2}^0, nn G_{1,2}^0$. LFV can be described in terms of three KM-type matrices K_{kL}, K_{kR} and W^l. Matrices K_{kL} and K_{kR} may be defined through charge-current Lagrangian,

$$\mathcal{L}_W^l = \frac{g}{\sqrt{2}}(\overline{e_{kL}}\gamma^\mu K_{kL}^\dagger n W_1^- + \overline{e_k}\gamma^\mu \frac{(1+\gamma_5)}{2} K_{kR}^\dagger n W_2^- + h.c.). \tag{2.19}$$

W^l is a combination of unitary matrices V_L and V_R connecting weak and physical charged-lepton fields, $W^l = V_R^{l\dagger} V_L^l$ ($l_{L,R}^W = V_{L,R}^l l_{L,R}$). The $K_{L,R}$ matrices satisfy relations $K_{L,R}^\dagger K_{L,R} = 1$ which lead to the GIM mechanism and assure the renormalizability of the models. All LFV vertices contain the matrix elements of CKM-type matrices or the matrix elements of their combinations.

2.3 Numerical estimation

The characteristic amplitudes that constitute all neutrinoless LFV amplitudes can be expressed in terms of several basic blocks, loop- or tree-level functions. These basic blocks have specific dependence on masses of intermediate particles and on the lepton flavor violation parameters from interaction vertices.
The lepton flavor violation parameters are defined in terms of the matrix elements of CKM-type matrices. Three important parameters are:

$$(s_L^{\nu_l})^2 = (K_L^\dagger K_L)_{ll}, \ (\ell = e, \mu, \tau) \tag{2.20}$$

For an approximate evaluation of any LFV amplitudes only these three parameters

are needed. The limits on this parameters are obtained by investigating the lepton flavor conserving processes experimentally. By studying the nonuniversality of the charge-current couplings in the lepton flavor conserving (LFC), deviations from unitarity of the CKM matrix and invisible width of the Z-bosons the following upper bounds on the $s_L^{\nu_l}$ were found,

$$
\begin{aligned}
(s_L^{\nu_e})^2 &< 0.0071 \\
(s_L^{\nu_\mu})^2 &< 0.0014 \\
(s_L^{\nu_\tau})^2 &< 0.03.
\end{aligned} \tag{2.21}
$$

In the model A the basic blocks are loop functions with the dependence on heavy neutrino mass. Further, the functions contain $s_L^{\nu_l}$ parameters. In the limit of the large heavy neutrino masses, the LFV amplitudes receive their maximal values.

In the model B the majority of neutrinoless processes in charged lepton decays contain tree-level Higgs-exchange amplitudes. These amplitudes consist of two fermion-Higgs vertices and an intermediate-Higgs propagator. The dominant contributions in the lepton-Higgs vertices and the quark-Higgs vertices are proportional to the heavy-neutrino masses and the quark masses, respectively. The heavy neutrino masses and non Standard Model (heavy) Higgs masses are both proportional to the left-right symmetry breaking scale v_R. Therefore contributions from the heavy Higgs to the leptonic amplitudes are independent of v_R, while the semileptonic amplitudes are proportional to the quark-mass to v_R ratios. The Higgs that corresponds to the Standard Model Higgs also contributes to the lepton flavor violating amplitudes, but each vertex connecting fermion to Standard Model Higgs contains an additional mixing factor κ_1^2/v_R^2, where $\kappa_1 \sim 250$ GeV is the $SU(2)_L \times U(1)$ breaking scale because the contributions to the amplitudes are strongly suppressed.

The upper bounds for $\tau \to \ell\ K^0$ are predicted to be

$$
\begin{aligned}
B_{th}(\tau \to e\ K^0) &= 9.8 \times 10^{-16} \\
B_{th}(\tau \to \mu\ K^0) &= 1.9 \times 10^{-16}
\end{aligned} \tag{2.22}
$$

from model A and

$$
\begin{aligned}
B_{th}(\tau \to e\ K^0) &= 1.1 \times 10^{-9} \\
B_{th}(\tau \to \mu\ K^0) &= 9.1 \times 10^{-10}
\end{aligned} \tag{2.23}
$$

from model B. A typical W-exchange box diagram is shown in Figure 2.1. n in this diagram represents for the heavy neutral lepton.

Another LFV processes with 3 charged particles are also predicted and summed up on Table 2.1.
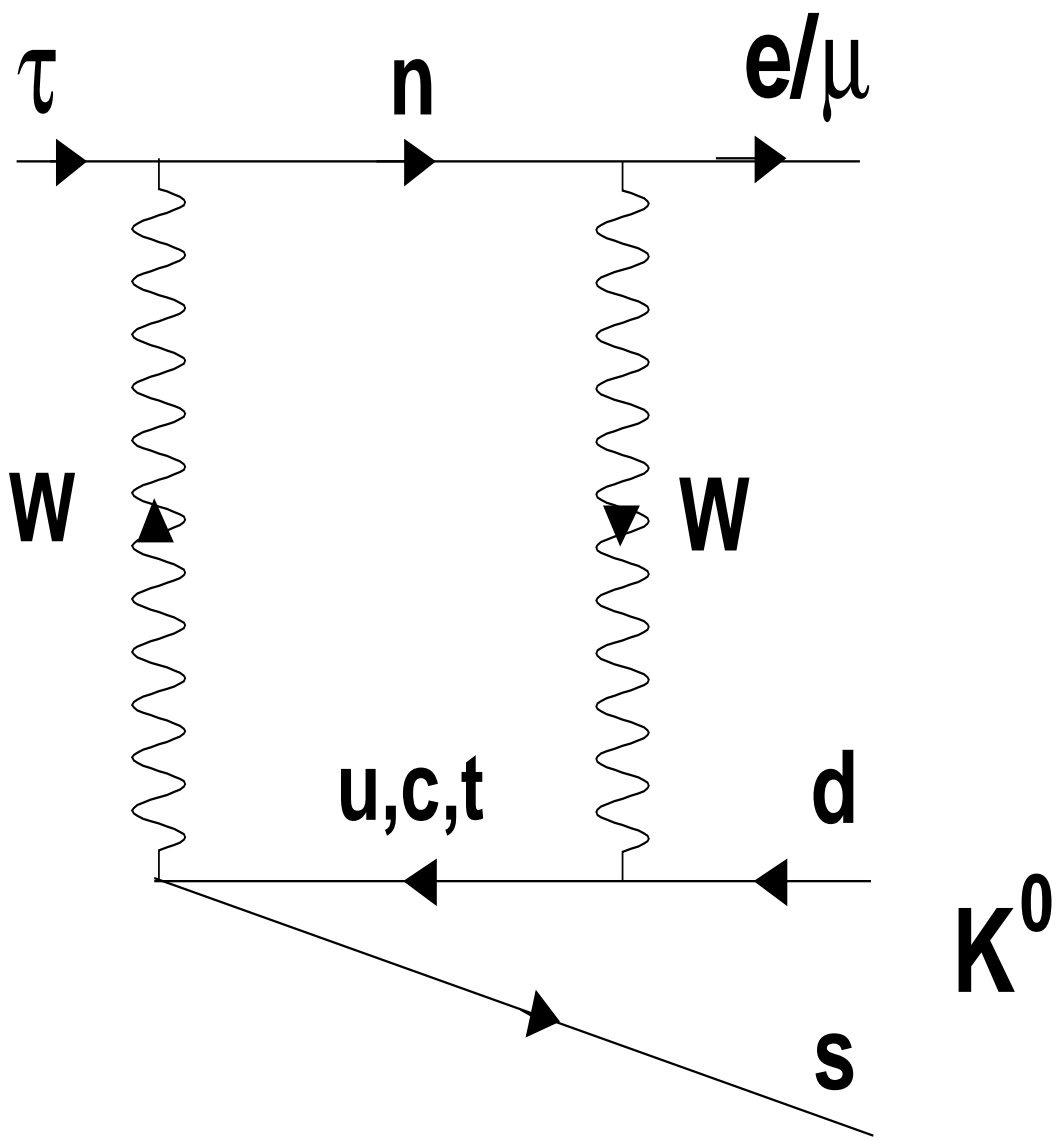
Figure 2.1: An typical Feynman diagram of $\tau \to \ell K^0$.

Process	Model A	Model B	Measured
$\tau \to e^- e^+ e^-$	2.7×10^{-6}	2.4×10^{-6}	2.9×10^{-6}
$\tau \to \mu^- \mu^+ \mu^-$	4.5×10^{-7}	4.0×10^{-6}	1.9×10^{-6}
$\tau \to e^- \mu^+ \mu^-$	1.4×10^{-6}	1.2×10^{-5}	1.8×10^{-6}
$\tau \to \mu^- e^+ e^-$	3.7×10^{-7}	1.4×10^{-5}	1.7×10^{-6}
$\tau \to e^+ \mu^- \mu^-$	1.3×10^{-9}	4.7×10^{-6}	1.5×10^{-6}
$\tau \to \mu^+ e^- e^-$	6.7×10^{-9}	2.0×10^{-5}	1.5×10^{-6}
$\tau \to e^- \pi^+ \pi^-$	2.7×10^{-6}	1.4×10^{-10}	2.2×10^{-6}
$\tau \to \mu^- \pi^+ \pi^-$	5.2×10^{-7}	1.2×10^{-10}	8.2×10^{-6}
$\tau \to e^- \pi^+ K^-$	3.3×10^{-15}	8.3×10^{-10}	6.4×10^{-6}
$\tau \to \mu^- \pi^+ K^-$	6.4×10^{-16}	7.1×10^{-10}	6.5×10^{-6}
$\tau \to e^- \pi^- K^+$	3.3×10^{-15}	8.3×10^{-10}	3.8×10^{-6}
$\tau \to \mu^- \pi^- K^+$	6.4×10^{-16}	7.1×10^{-10}	7.4×10^{-6}
$\tau \to e^- K^- K^+$	1.1×10^{-6}	6.9×10^{-9}	6.0×10^{-6}
$\tau \to \mu^- K^- K^+$	2.1×10^{-7}	6.0×10^{-9}	15×10^{-6}
$\tau \to e^- \rho^0$	2.7×10^{-6}		2.0×10^{-6}
$\tau \to \mu^- \rho^0$	5.3×10^{-7}		6.3×10^{-6}
$\tau \to e^- K^*(892)^0$	2.4×10^{-15}		5.1×10^{-6}
$\tau \to \mu^- K^*(892)^0$	4.7×10^{-16}		7.5×10^{-6}
$\tau \to e^- \bar{K}^*(892)^0$	2.4×10^{-15}		7.4×10^{-6}
$\tau \to \mu^- \bar{K}^*(892)^0$	4.7×10^{-16}		7.5×10^{-6}
$\tau \to e^- \phi$	2.3×10^{-6}		6.9×10^{-6}
$\tau \to \mu^- \phi$	4.5×10^{-7}		7.0×10^{-6}

Table 2.1: The calculated upper bounds and measured Upper limits [6] of the branching fractions for lepton flavor violating processes. Model A and B correspond to the Models we mentioned in Chapter 2.

Chapter 3

KEK B-factory

The measurement of CP violation is main subject of BELLE experiment. The KEKB accelerator and Belle detector are optimized to satisfy the physics reqirement of the CP violation studies. But they are useful for the study of τ physics. In this chapter, we give the description of the KEKB accelerator, Belle detector and the software system we used in the experiment.

3.1   KEKB accelerator

KEKB accelerator, located in Tsukuba, Japan is an asymmetric high luminosity e^+e^- collider. The accelerator is designed to have two separate rings for e^+ and e^- beams because each of them has defferent beam energy. They are located in the TRISTAN tunnel as shown in Figure 3.1. e^+ and e^- beams are accerelated by linear accelerator and injected into main ring at Fuji area. The e^+ beam circulates with the energy of 3.5 GeV in low energy ring (LER) anti-clockwise, and the e^- beam circulates with the energy of 8.0 GeV in high energy ring (HER) clockwise. Both of the orbit length are about 3 km. The RF cavities which make up energy to the beams are instsalled at Nikko and Oho area for HER and at Fuji area for LER. The rings are crossing at Tsukuba and Fuji experimental hall. The beams are made collide at the interaction point in the Tsukuba experimental hall, where the Belle detector is furnished.

The center of mass energy $\sqrt{s}$ is 10.58 GeV. This is equal to the invariant mass of $\Upsilon(4S)$ which decays into $B\bar{B}$ pairs mainly. At this energy region, τ pairs are created from e^+e^- in QED processes with the cross section of 0.91 nb. This is almost same number of $\Upsilon(4S)$ event, so that we can get τ samples as many as $B\bar{B}$.

The designed value and achieved record of KEKB parameters are listed in Table 3.1. A unique feature is that e^+e^- collide at a small angle θ_x in order to reduce parasitic collision near the IP. In December 2001, the peak luminosity achieved to 5.4×10^{33} /cm^2/s, the half of the design value, but highest in the world. The beam currents was 1.2 A for the LER and 0.8 A for HER. The achieved LER current is much lower than design value. This is because the positron bunch is blown up by the background electron in the beam pipe. To avoid this defect, we set the coils around

Parameters	LER	HER	Units
Particles	e^+	e^-	
Energy (E)	3.5	8.0	GeV
circumstance (C)	3016.26		m
Luminosity (L)	5.466×10^{-33} (1×10^{-34})		$\text{cm}^{-2}\text{s}^{-1}$
Crossing angle (θ_x)	± 11		mrad
Tune shifts (ξ_x/ξ_y)	0.039/0.052		
Beta function at IP (β_x^*/β_y^*)	0.33/0.01		
Beam current (I)	1.2 (2.6)	0.8 (1.1)	A
Natural bunch length (σ_z)	0.4		cm
Energy spread (σ_E/E)	7.1×10^{-4}	6.7×10^{-4}	
Bunch spacing (s_B)	0.59		m
Particles/bunch	3.3×10^{10}	1.4×10^{10}	
Emittance (ϵ_x/ϵ_y)	$1.8 \times 10^{-8}/ 3.6 \times 10^{-10}$		m

Table 3.1: Parameters of KEKB (number in the brakets are design value.)

the LER beam pipe to attract the electron to the wall of the pipe. According to this operation, we are able to set high LER current without making the positron bunch size larger.

3.2 Belle detector

The figure 3.2 show the overview of Belle detector. The Belle detector makes precise measurements of charged and neutral particles, decay vertex, momentum, energies and particle identification. The detector components dedicated for Belle experiment are a sillicon vertex detector (SVD)[12], a central drift chamber (CDC)[13], an array of 1188 aerogel Čerenkov counter (ACC)[14], 128 time-of-flight scintillation counters (TOF)[15], and an electromagneticcaloriemeter containing 8736 CsI(Tl) crystals (ECL)[16], all located inside the suprerconducting solenoid that generates a 1.5 T magnetic field. An iron return yoke outside the solenoid is segmented into 14 layers of 4.7-cm-thick iron plates alternating with a system of resistive plate counters that is used for identification of muons and detection of K_L^0 mesons (KLM)[17], and an extreame forward caloriemeter (EFC) containing 160 BGO($Bi_4Ge_3O_12$) crystals in each endcap is placed around the beam line. Brief descriptions of the sub-detectors are given in the following subsections. Note that the coordinate system used in this dissertation is drfined as Figure 3.3.
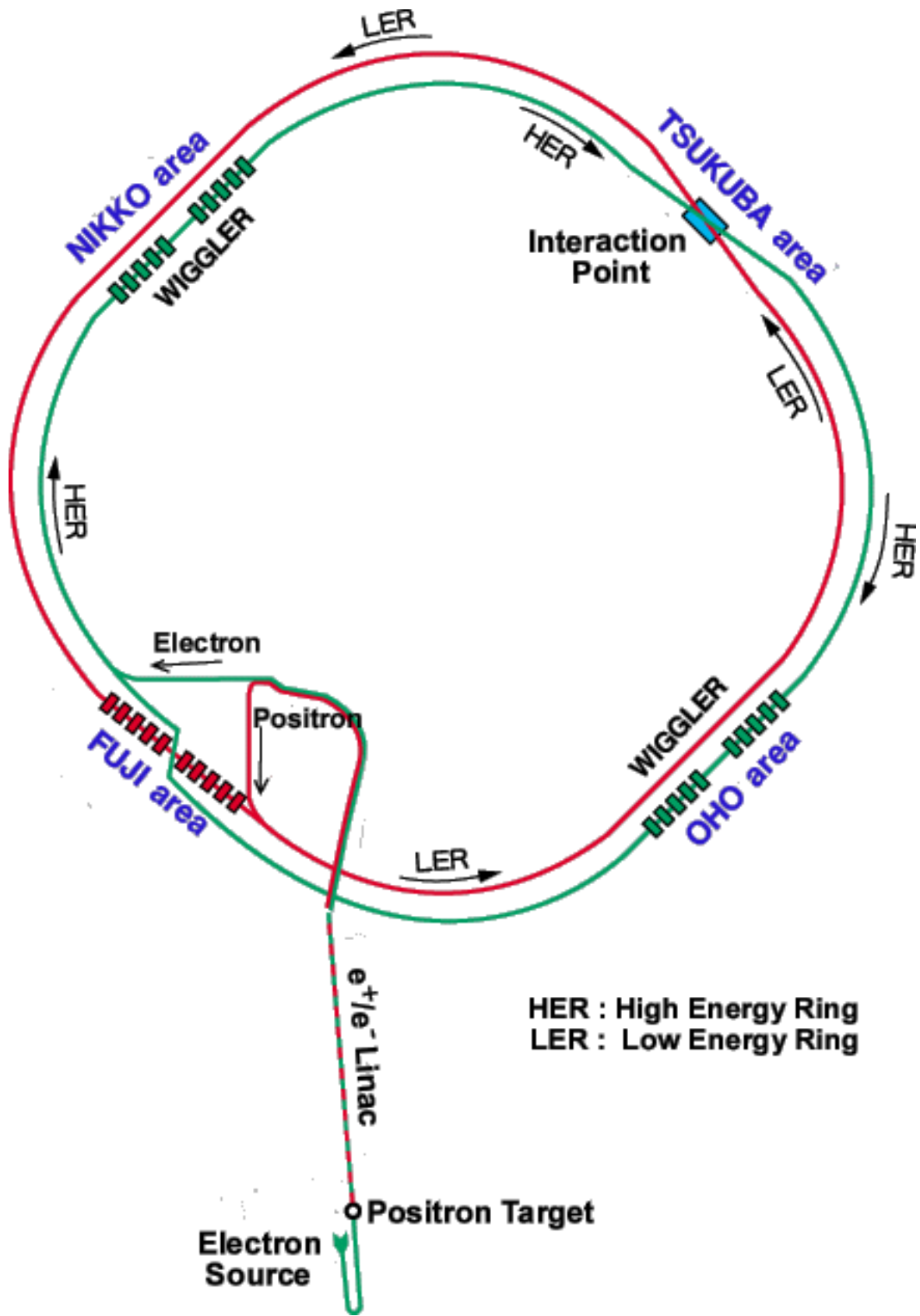
Figure 3.1: Configuration of the KEKB strage ring.
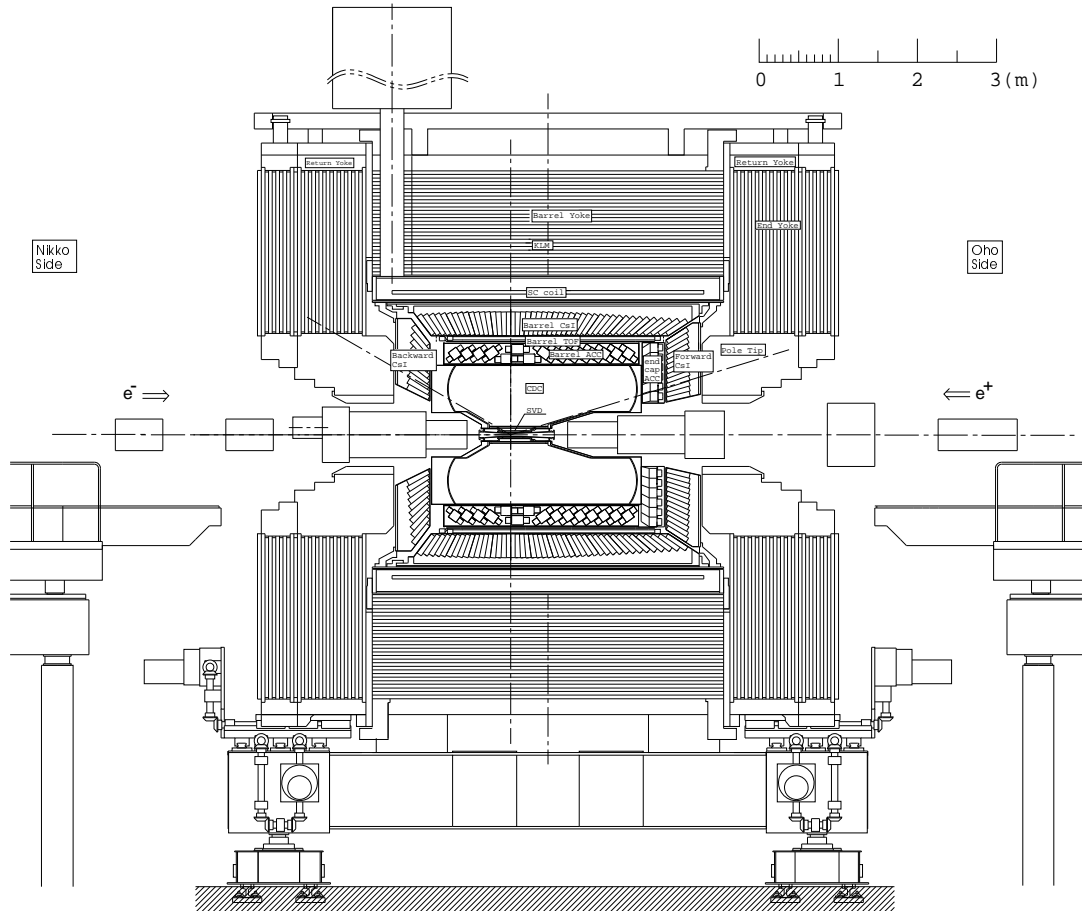
Figure 3.2: Sideview of Belle detector.
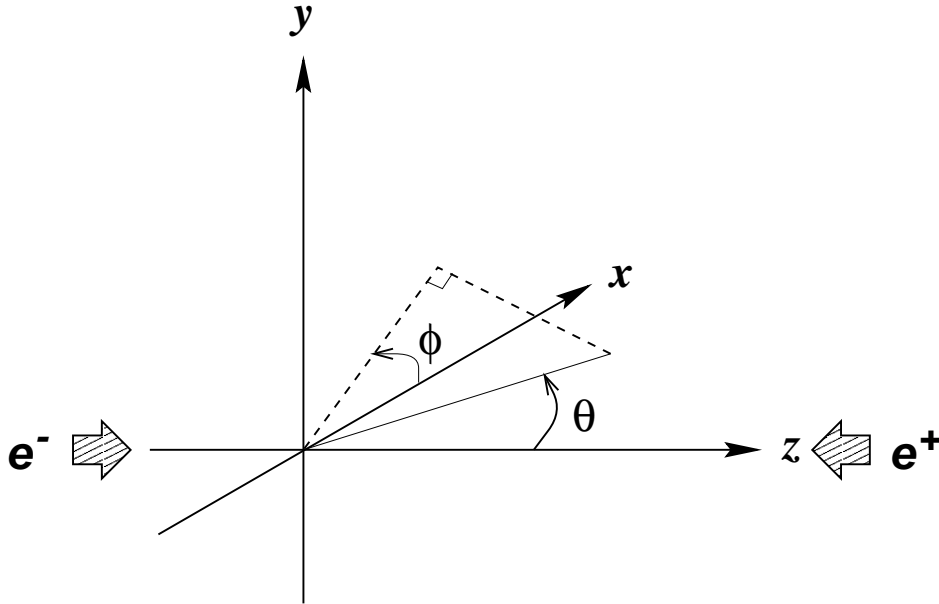
Figure 3.3: Definition of Belle coordinate system.

3.2.1 Silicon Vertex Detector(SVD)

The SVD measures charged track points with position resolution of about 10 μm. The tracking is done with a combination with hit points from the CDC. The SVD comprises three layers of the 300-μm-thick double sided silicon detector (DSSD) ladders, each consists of 8, 10 and 14 ladders from the inner to the outer layer. Each DSSD has orthogonal strips in rach sides and provides two orthogonal measurements along ϕ and z directions. Figure 3.4 shows the configuration of SVD. The SVD occupies the region from 20.5 mm to 75 mm in radius, and from -150 mm to 220 mm in z component, and the acceptance in polar angle is $20° < \theta < 150°$. A more detailed description of the SVD and its performance is given in Ref. [12].

3.2.2 Central Drift Chamber (CDC)

The role of the CDC is to measure the track positions, momentum and specific ionization (dE/dx) of charged particles. The dE/dx information is used for the particle identification, and combined with other particle identification from the detectors (ACC/TOF). In addition, another indispensable role of the CDC is to provide an online hardware trigger (so called "Level 1 trigger"). So far, only the CDC can provide a trigger for events which come from near the IP.

The CDC is a small-cell drift chamber containing 50 anode layers (32 axixl and 18 stereo wire layers) and 3 cathode strip layers. The anode layers are grouped into 11 superlayers (6 axial and 5 stereo superlayers). Combining axial and stereo hit
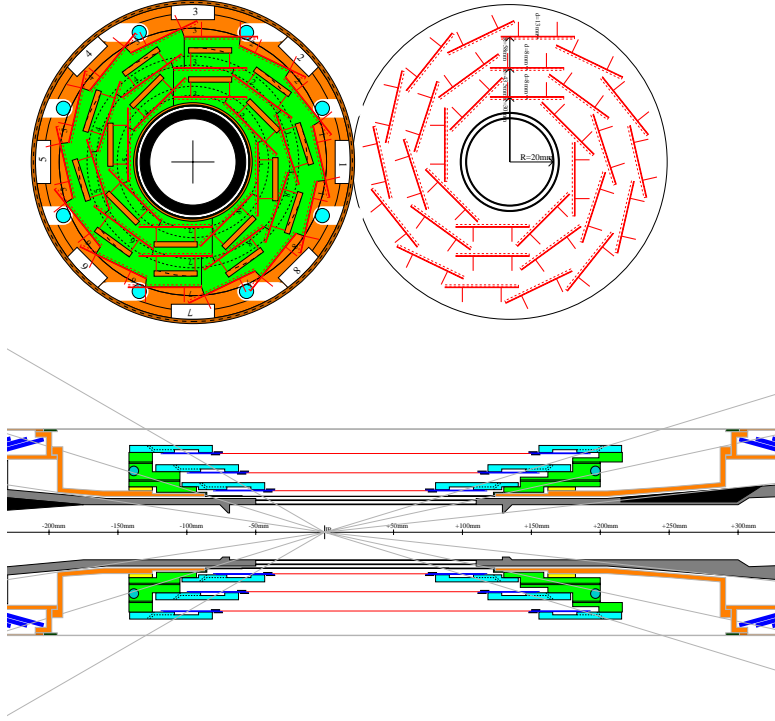
Figure 3.4: Silicon vertex detector.

information, 3-demensional track reconstraction becomes possible. The cathod layers are located at the most inner part of the CDC, which measure the z position of charged tracks. The number of readout channels is 8400 for anodes and 1792 for cathod in total. Figure 3.5 shows the geometrical configuration of the CDC. The CDC covers the region of 77 mm to 880 mm in radious and $17°$ to $150°$ in polar angle. Low Z-gas(50% He and 50% C_2H_6) is used to reduce multiple scattering of a charged particles. In spite of low Z-gas, a good dE/dx resolution is due to a large content of ethane.

The spacial resolution is 130 μm in $r - \phi$ plane and less than 2 mm in z, which leads the transverse momentum resolution σ_{p_t}/p_t of $\sqrt{(0.19p_t)^2 + (0.34)^2}\%$ where p_t is the transverse momentum in unit of GeV/c. The dE/dx resolution is 6.9% for minimum ionizing particles. A more detailed description is given in Ref. [13].

3.2.3 Aerogel Čerenkov Counter (ACC)

The ACC provides an information to separate charged kaons from charged pions in high momentum range (1.2 GeV/c < p < 3.5 GeV/c), which extend the reach of TOF. The ACC is an array of threshhold type silica aerogel Čerenkov counters. It consists of two part; barrel and endcap.

15

CDC structure

CFRP 5mm^t

R880mm

Al 10mm^t

150°

760mm

1590mm

17°

R275mm

IP

Figure 3.5: Central drift chamber.

The barrel part consists of 960 aerogel counters that are segmented into 16 divisions in z and 60 in ϕ. The aerogel refractive index varies with the poler angle ($n = 1.01$, 1.013, 1.015, 1.020 and 1.028) and has been optimized to match the kinematics of two-body decays from the boosted B mesons. Figure 3.6 shows the 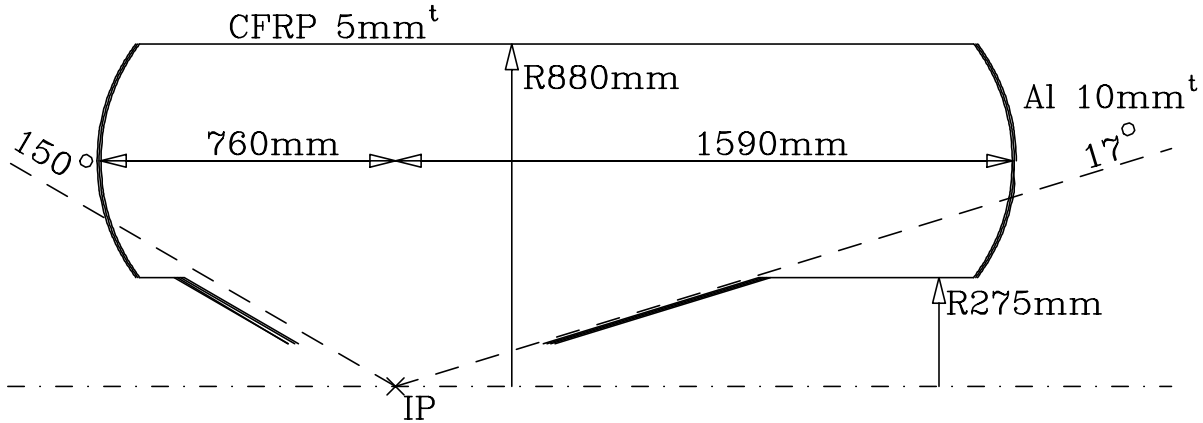configuration of barrel ACC. The Čerencov light from each barrel counter is fed into one or two fine-mesh photo-multipliers (FM-PMT) which can work in the 1.5 T magnetic field through air lightguides. The number of readout channels for the barrel ACC is 1560 in total.

The endcap ACC is placed only in the forward side. It consists of 228 counters with $n = 1.03$. The counters are mounted in five concentric rings with different radii. Each ring contains 36, 36, 48, 48 and 60 counters from inner to outer. Each endcap counter has one FM-PMT for readout and therefore the number of readout channels is 228. Figure 3.7 shows the configuration of endcap ACC. A more detailed description of the ACC and its performance is given in Ref. [14].

3.2.4 Trigger/Time of Flight counter (TSC/TOF)

The TOF is used to distingush charged kaons from charged pions in the low momentum region ($p < 1.2$ GeV/c). The Trigger Scintillation Counter (TSC) together with the TOF generates the primary timing signal for the Level 1 trigger.

The configuration of TOF/TSC module is shown in Figure 3.8. Two trapezoidally shaped 4 cm-thick TOF scintillators and one 0.5 cm-thick plate TSC scintillator form one module. In total 64 modules are placed at 1.2 m from IP and covor $34° < \theta < 120°$. TOF information is read out by FM-PMTs at both ends of scintillators, while TSC is read out by single FM-PMT from the backward end. The total number of readout cannels of TOF is 320. The detail of the TOF is given in Ref. [15].

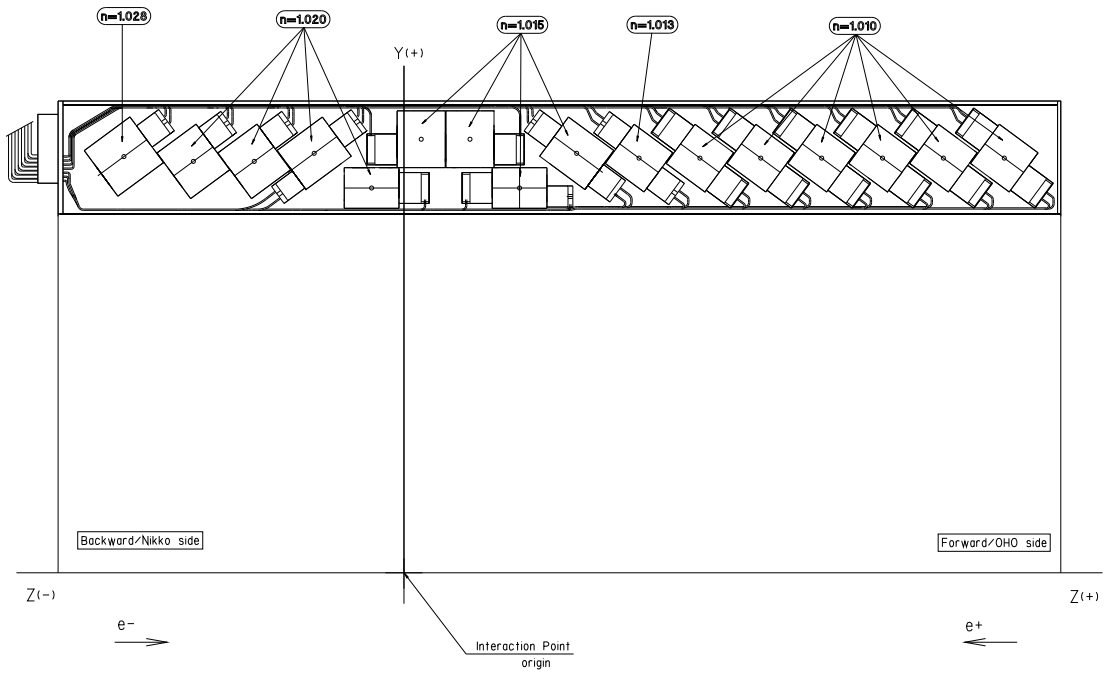16

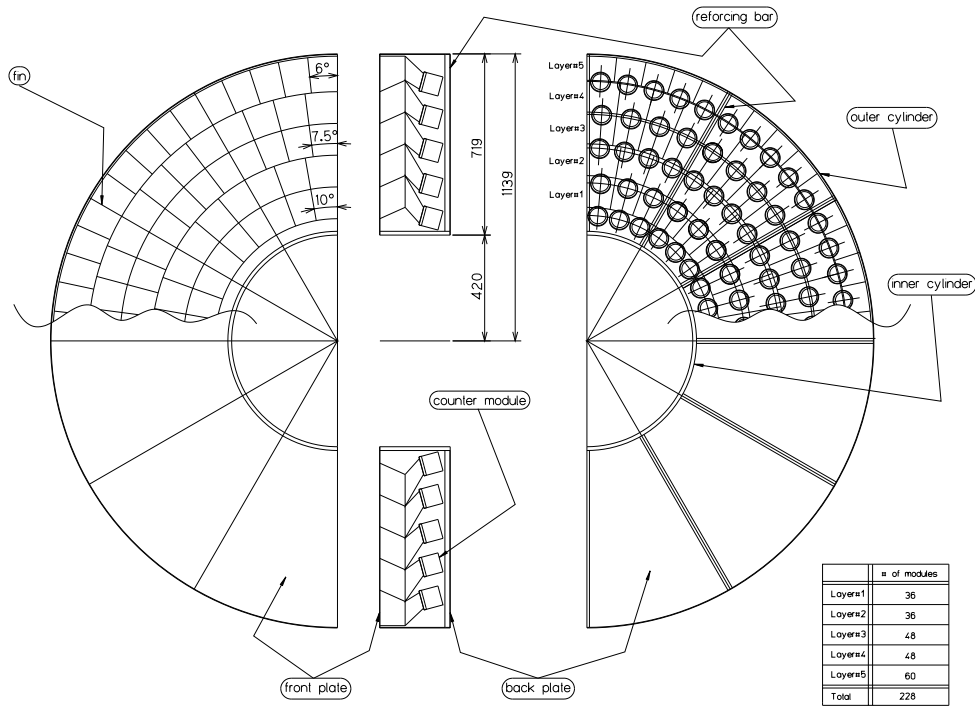Figure 3.6: Barrel aerogel Čerencov counter.

	# of modules
Layer#1	36
Layer#2	36
Layer#3	48
Layer#4	48
Layer#5	60
Total	228

Figure 3.7: Endcap aerogel Čerencov counter.

17
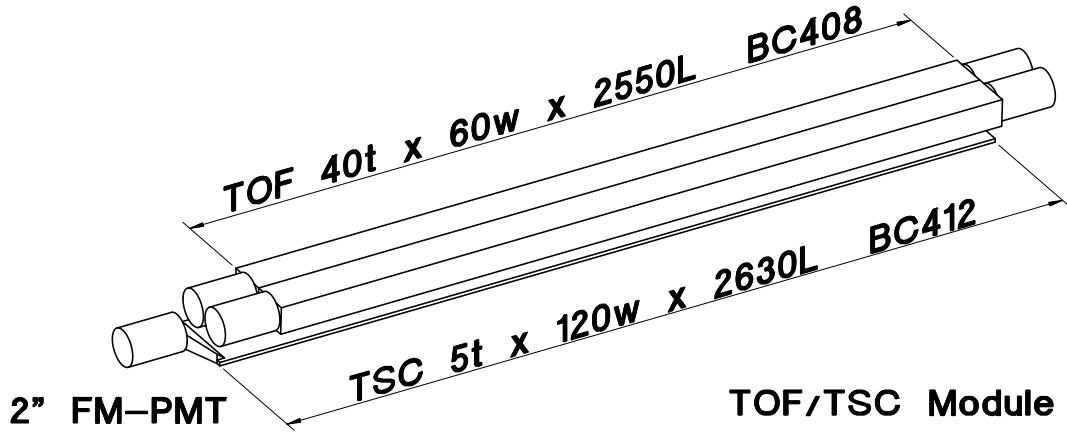
Figure 3.8: Time of flight and trigger scintillator counters.

3.2.5 Electromagnetic Calorimeter(ECL)

The ECL measures the energy deposit of particles using the scintillation light from electromagnetic shower which charged and neutral particles generate in the CsI(Tl) crystals. Photons deposit most of their energy in the crystals, thus we can measure the energy of the photons. Electrons also deposit large energy that we can consider the tracks which has good agreement with ECL hits are electron. The ECL provides various triggers and also provides the secondary timing signal for the L1 trigger.

Figure 3.9 shows the configuration of the ECL. The ECL consists of total 8736 CsI(Tl) crystals. The barrel part is installed at the radius of 125 cm from IP and covers the polar angle region of $32.2° < \theta < 128.7°$. The forward and backward endcap ECL are placed at $z = 196$ cm and -102 cm and covers $12.01° < \theta < 31.36°$ and $131.5° < \theta < 155.0°$ respectively. The 6624, 1152 and 960 crystals with two 2cm × 1 cm photodiodes for read out are filled in barrel, endcap forward and endcap backward modules respectively.

The energy resolution measured by a photon beam test with the threshold energy of 0.5 MeV and with the 5 × 5 crystal matrix is $\sigma_E/E = 0.066\%/E \oplus 0.81\%/E^{1/4} \oplus 1.34\%$ and the position resolutuin is $\sigma_{pos} = 0.5$ cm$/\sqrt{E}$, with the unit of E in GeV. The detail of the ECL is given in Ref. [16].

3.2.6 K_L/μ detector (KLM)

The KLM detector is designed to identify the K_L mesons and muons in a broad momentum range above 600 MeV/c. The KLM consists of alternating layers of glass resistive plate counter (RPC) filled up with the gas mixture (30 % argon, 8
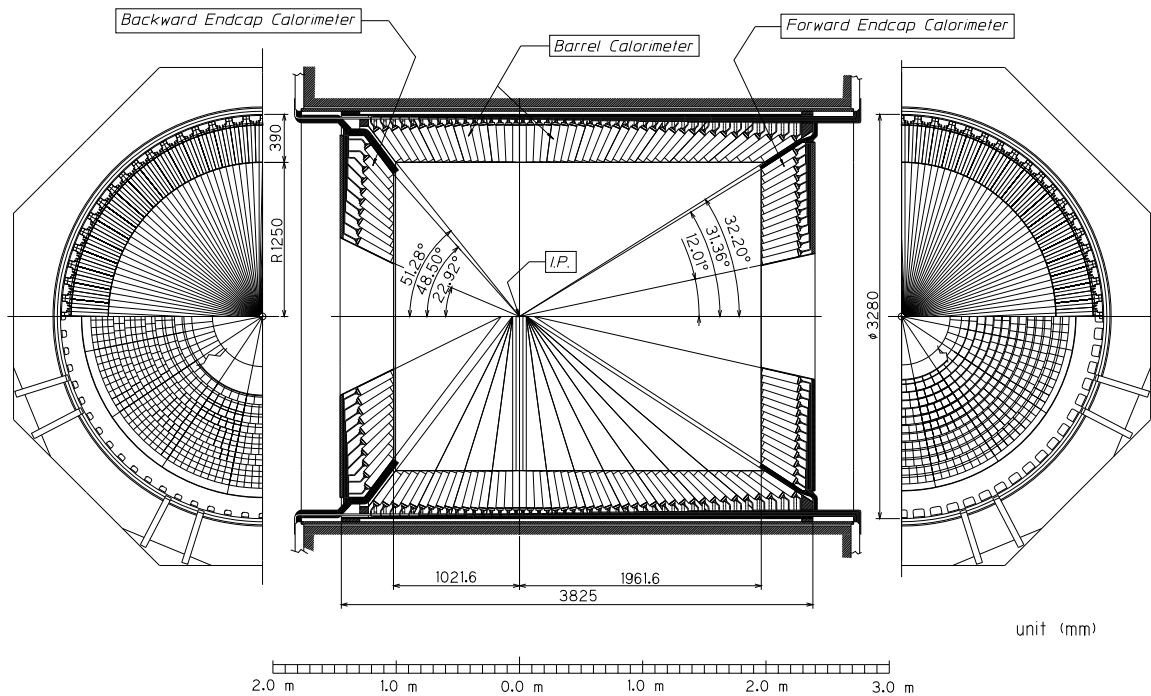
Figure 3.9: Electromagnetic caloriemeter

% butane and 62 % HFC134a) and 4.7 cm-thick iron plates. The high voltage is applied to the glass plate electrodes. When charged particles go through the ionize gas in the RPC, the amplified signals is picked up by the strips sticked outer side of glasses. The K_L mesons interact with iron and give a small hadron shower that we can detect. Muon lose energy only through ionization. On the other hands, hadrons interact stlongly with the iron and scatter usually without managing to penetrate more than a few KLM layers. Thus we can separate muons from hadrons.

Figure 3.10 and 3.11 show the configuration of the barrel and endcap KLM respectively. The KLM consists of an octagonal barrl detector and two endcap detectors that are diveded into quadrant part of modules. The barrlel mdules are rectangular in shape and vary in size from 220×151 to 220×267 cm^2. The endcap modules are in fan shape of the inner radius of 130.5 cm, and the outer radius of 331 cm. The KLM covers the polar angular region of $25° < \theta < 145°$. The number of read-out cannels of KLM is 21856 in barrel and 16128 in endcap. From the cosmic ray measurement, we estimate the angular resolution of hit point from the IP is better than 10 mrad and the time resolution of KLM system is $\sim$ sevral nsec. The detail of the KLM is given in Ref. [17].

19
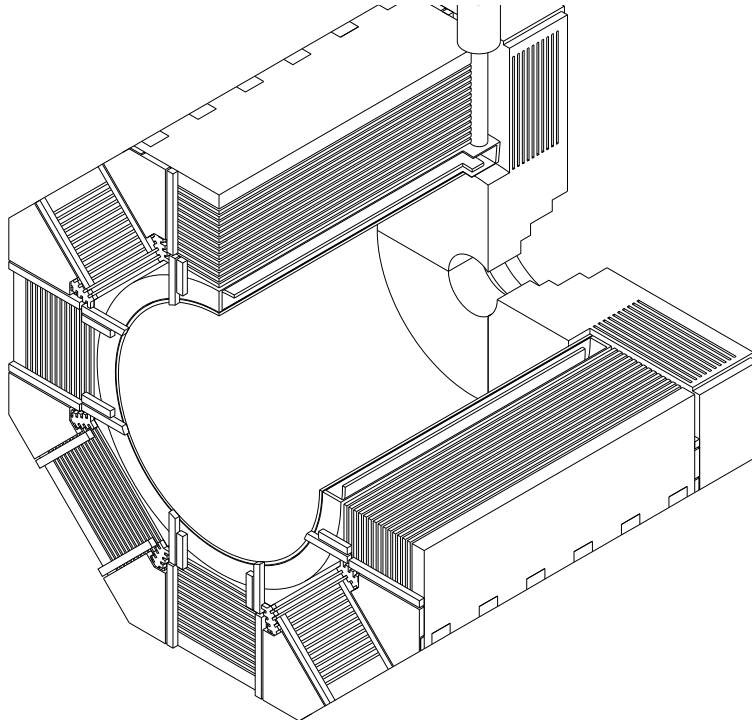
Figure 3.10: Schematic view of barrel KLM.
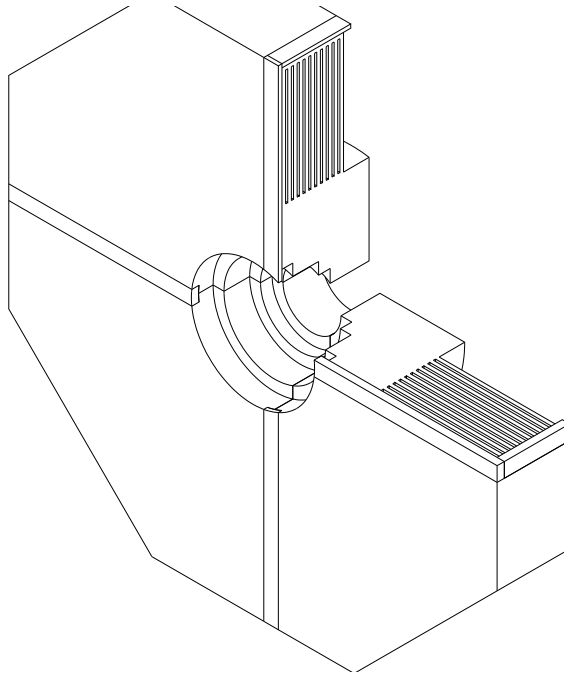
Figure 3.11: Schematic view of endcap KLM.
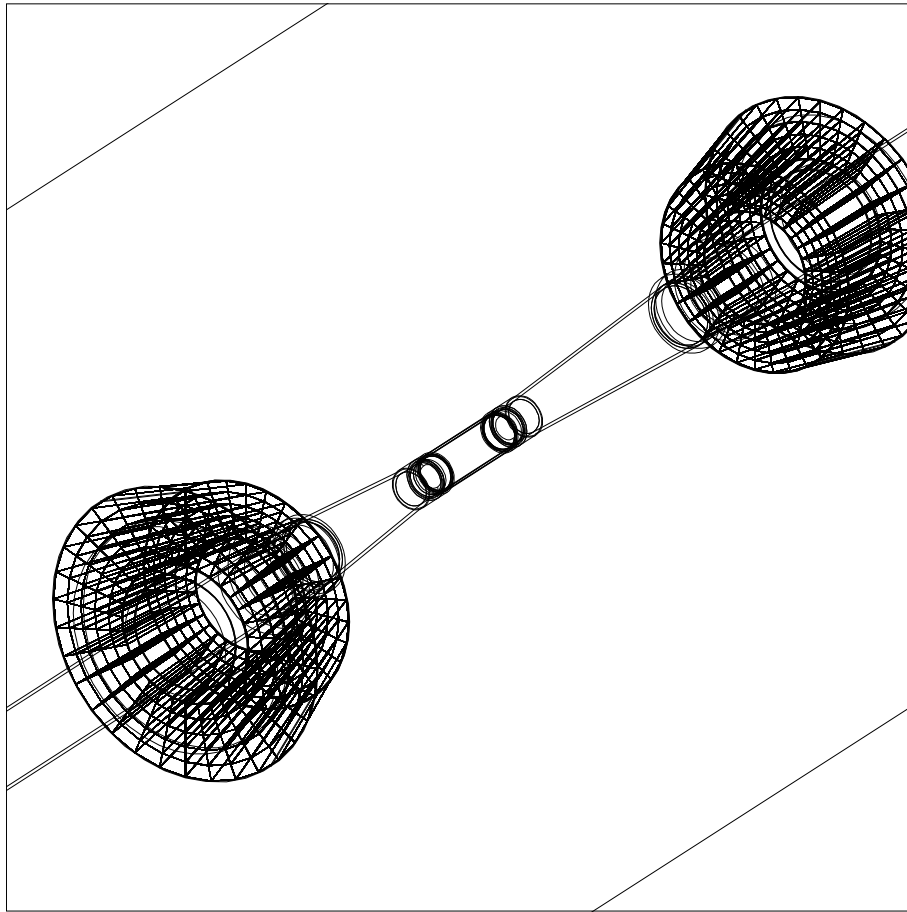
Figure 3.12: Extreme forward caloriemeter.

3.2.7 Extreme Forward Calorimeter (EFC)

The EFC measures the energy of photons and electrons at the extreme foward and backward direction out of the ECL acceptance. We use BGO ($Bi_4Ge_3O_12$) crystals because the EFC is exposed in high irradiation (about 5 MRad/year) of photons from the syncrotron radiation and the spent electrons. EFC is installed attached to the front faces of the cryostats of the compensation solenoid magnets of the KEKB storage ring, sorrounding the beam pipe as shown in the Figure 3.12. More detail of the EFC is discribed in Ref. [18].

3.2.8 Trigger and Data Acquisition system (DAQ)

Trigger system

In order to record the data of physics events of our interest, we have to provide the common stop signal for TSC's and the gate signal for ADC's. Figure 3.13 shows the logic diagram of the trigger system. We combine sub-triggers from sub-detectors in
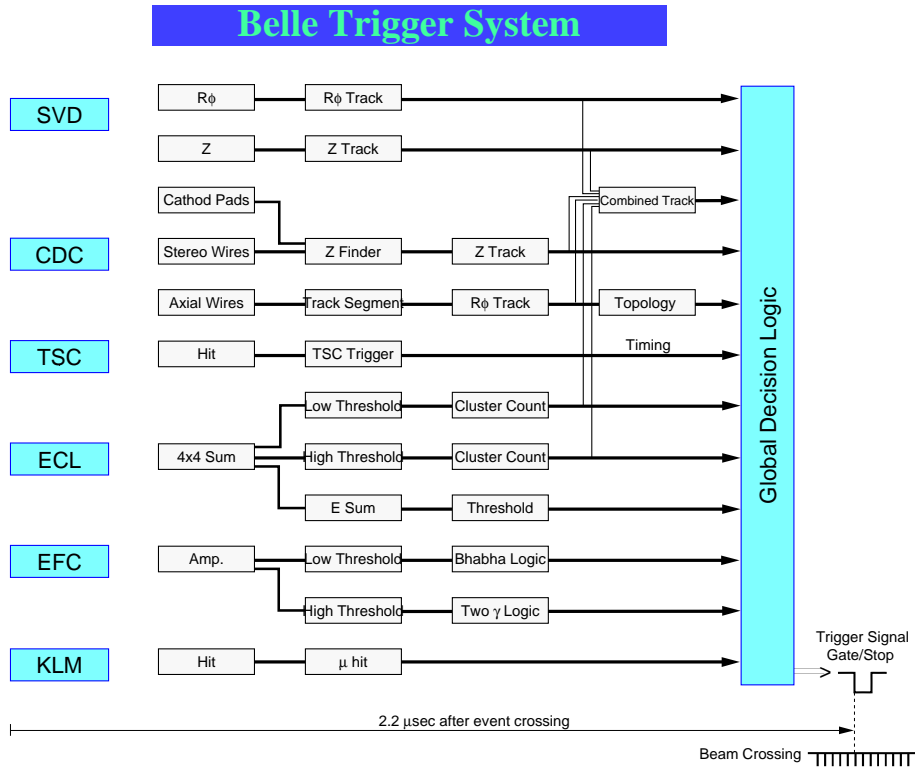
Figure 3.13: Logic diagram of Belle trigger system

what we called the Global Design Logic (GDL) and form the master triggers. A decision for the triggers is made within 2.2 μs after the beam collision at the IP. Typical trigger rate was 200 Hz,with which the DAQ deadtime is about 4 %.

Data Acquisiyion system

In order to achieve the data acquisiyion with a deadtime fraction less than upto 500 Hz of trigger rate, a distributed-parallel DAQ system has been devised. A schematic view of the Belle data acquisition system is shown in Figure 3.14. The subsystem for readout from sub-detectors and also from the trigger systems run in parallel. We adopt a charge-to-time(Q-to-T) conversion frontend electronics, except for KLM which provides the time-multiplexed information on a signal line. The data from each subsystem are combined into a single event recorded by the event builder which converts the "detecter-by-detector" parallel data streams to "event-by-event" river. The event builder output is transfered to the online computer farm. The online farm consists of 120 processors for the fast reconstraction of up to 15 MBytes/sec event data stream. After passing the computer farm, the events are stored into the mass storage system and eventually stored into the tapes for off-line use.
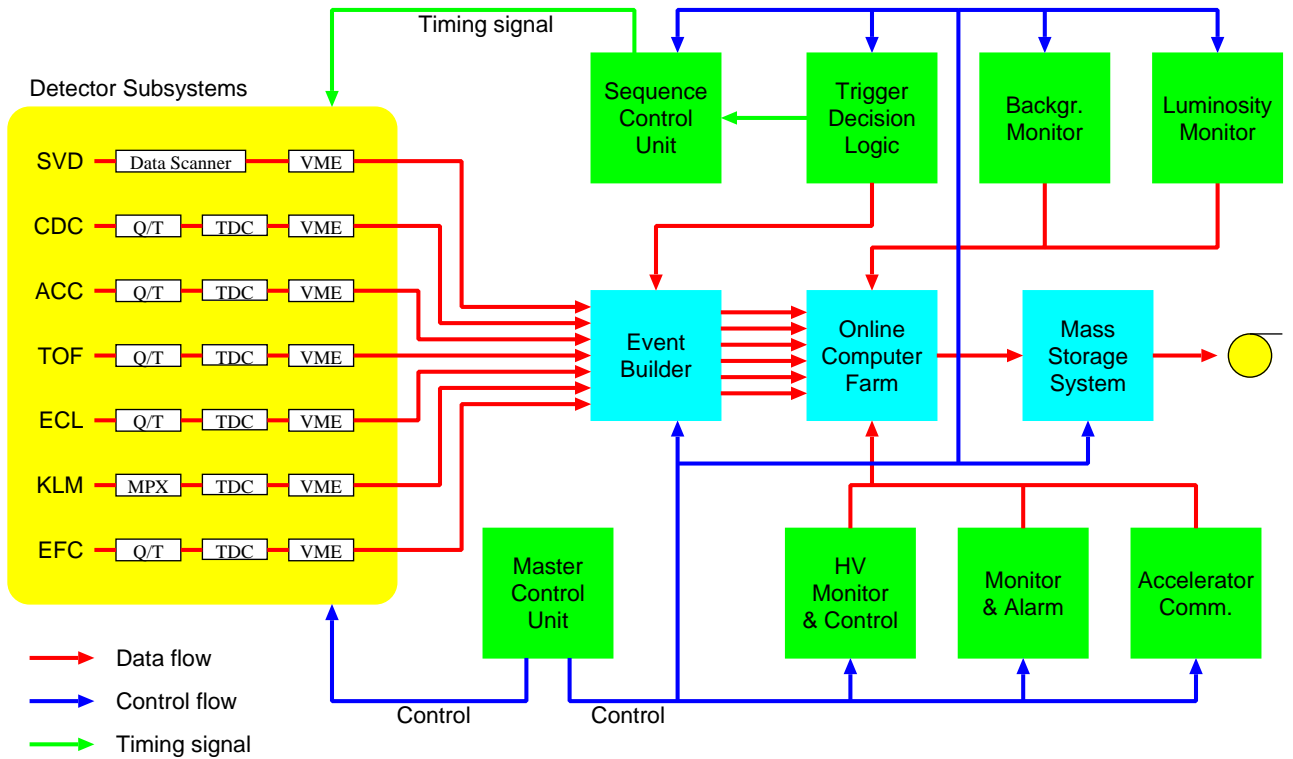
Figure 3.14: Logic diagram of Belle Data Acquisiyion system

3.3 Software

We give a brief overview of the structure of the analysis environment and the description of Monte Carlo simulation program optimized to the Belle experiment.

3.3.1 Overview

The raw data taken by the DAQ are processed in off-line using sevral kinds of reconstraction tools. The hits in the SVD and CDC are associated by the charged particle tracker. The energy management converts the information from ECL to the energy and flight direction of photons.The particle identification (PID) tools provide the inforamation about the kind of the particles. These inforamation from reconstruction tools are stored into Data Summarry Tape (DST) . For the physics analysis, DSTs are so large that we convert it more convenient and compact subset of data (Mini-DST).

To manage MDSTs and get the final result, analysis and simulation tools consist of many program modules which are executed on a common frame work so called "BASF".

3.3.2 Monte Carlo simulator

For Monte Carlo simulation, we have two detector simulators. One is the fast simulator and the other is the full detector simulator. The fast simulator (FSIM) uses the parameterized detector performance, and generate MDST data directry. The FSIM does not need so much CPU power, but can not simulate detailed environment as to the detector resolution and so on. It is great advantage to save CPU time, so that we can simulate enormous number of interaction between the particles from the event and our detector. We use GEANT [19] based full detector simulator (GSIM) in this analysis. When we input the event, the GSIM geneates detector response. Data generated by GSIM is processed by the reconstraction tools, and subsequent process is the same as real data. For Monte Carlo event generation, we use three kind of generators. For τ pair event generation, KORALB [20] event generator is used. The KORALB was developed for the τ pair production process at low energies, $\sqrt{s} < 30$ GeV. We use on the other hands, QQ [21] event generator for background of hadronic event ($B\bar{B}$ and $q\bar{q}$ for continuum). The QQ was developed for study of B mesons in the $\Upsilon(4S)$ resonance. Both of generators are developped by CLEO collaboration so that designed for a symmetric collider, they have been adjusted to describe the Belle experiment. Also for the background estimation, we use the aafhb generator [22] for the two photon process. The aafhb is the modified from the aafh generator for BELLE. The aafh calculates the four-fermion production from e^+e^-collisions. The decay table which controls the decay of generated particle is described according to the latest decay branching fractions by Particle Data Groupe (PDG) [23]. We can modify the table and define the decays and its decay products. We generate Monte Carlo of $\tau \to \ell K^0$ events (signal events) using KORALB and modify decay table in assumption of the uniform angular distribution of the τ decay in the rest frame of τ.

Chapter 4

Analysis

In this chapter, we describe the method and results of this analysis.

4.1   The data set

The analysis is performed with the data of Experiment 7 to 13 (January 2000 - July 2001) runs collected with Belle detector. The total integrated luminosity is 29.4 fb^{-1}. This corresponds to 26.8×10^6 τ pair events. A large part of the data was taken under the condition of the total beam energy W = 10.58 GeV to be in the region of $\Upsilon(4S)$ resonance. Some part of the data is taken at the energy 30~60 MeV below the $\Upsilon(4S)$ resonance, for background study of B-physics. We call former as "on-resonance" data and later as "off-resonance" data. The data we analyzed contains 2.6 fb^{-1} off-resonance data. The cross section of τ pair creation does not change both of the condition, so we treat the off-resonance data as same as on-resonance data.

For background study, we use Monte Carlo events of 40×10^6 generic $B\bar{B}$, 79×10^6 generic uds (combination $u\bar{u}, d\bar{d}, s\bar{s}$ continuum), 39×10^6 generic $c\bar{c}$, 50×10^6 generic τ pair, each 100×10^6 $ee \rightarrow eeee$, $ee \rightarrow ee\mu\mu$, $ee \rightarrow eeuu$, 50×10^6 $ee \rightarrow eess$ and 1×10^6 $ee \rightarrow eecc$ samples. They are large enough comparing to the data size of this analysis.

For signal events, we use 100000 τ-pairs which one τ decays into ℓ K^0 and the other τ decays into a generic mode.

4.2   Event selection

We set the event selection criteria by studying the signature of $\tau \rightarrow \ell$ K^0 event. First, We require the τ pair event selection criteria that was used generally in Belle. The event topology, good quality K_S, lepton and kinematics of the candidate system must be consistent with that of signal. We optimized the cut parameters using the signal Monte Carlo.

4.2.1 τ pair event selection

- $2 \leq$ No. of good tracks ≤ 8
- $\Sigma P^* < 10$ GeV/c
- $\Sigma E(ECL) < 10$ GeV
- $|\Sigma(\text{charge})| \leq 2$
- Ptmax > 0.5 GeV/c
- $E^*_{rec} > 3$ GeV or Ptmax > 1 GeV/c
- $E^*_{tot} < 9$ GeV or $\theta_{max} > 175°$
- No. of tracks in barrel region ≥ 2 or $E(ECL_{trk}) < 5.3$ GeV
- $\theta_{max} > 20°$

where

- $\cdot$ * denotes a center of mass (CM) system of e^+e^- collision,
- $\cdot$ "Σ" represents the summation in an event,
- $\cdot$ Ptmax: maximum transverse momentum,
- $\cdot$ $\theta_m ax$: maximum polar angle,
- $\cdot$ good charged track: Pt ≥ 0.1 GeV/c, helix $|dr| < 3$ cm, $|dz| < 5$ cm,
- $\cdot$ E^*_{rec}: Sum of energies of all charged tracks and energies of all gamma,
- $\cdot$ E^*_{tot}: Sum of E^*_{rec} and magnitude of the missing energy,
- $\cdot$ $E(ECL_{trk})$: Sum of the energy of ECL hits without gamma.

These are the τ pair event selection criteria we used generally at BELLE. The main motivation of these cuts is to separate τ pair events from hadronic event and to reject the background events from Bhabha and two photon processes. The signature of τ pair events is to be low multiplicitiy and to have missing energy that is caused by neutrino emission at τ decay. Bhabha events have quite a narrow 2 jet event shape. Two photon processes have missing energies toward almost same direction as e^+e^- beams. The cuts are defined to reflect these features.
In addition, we require the summation of perpendicular momentum of all tracks and photons in each events are larger than 0.2 GeV/c. This requirement is so loose that most of signal events are saved, but Bhabha events rejected well.

4.2.2   Event topology

For each candidate event we require having well reconstructed charged particles of $2 \sim 4$ and at least one K_S candidate. In the CM system of the e^+e^-, τ pairs are produced back-to-back. Each τ has an energy of 5.29 GeV. τ decays mainly into 1-prong with branching ratio of 85%, so that we select events with one τ decaying

into a 1-prong final state and the other (signal) τ decaying into a 1-prong and 1 V-shape event in the final state. The candidates are in a 1-prong-vs-3-prong topology. The event topology is determined by defining a plane perpendicular to the thrust axis that is calculated by all charged tracks, and counting track and Vee candidates on either side of the plane.

4.2.3 K_S selection

We select K_S^0 candidates from Vee particle candidates on DST table so called "*Mdst_Vee2*". We introduce the following parameters for selection of $K_S^0(\to \pi^+\pi^-)$ candidates,

- dr: The smaller impact distance from the IP to the two tracks in x-y plane,
- $d\phi$: The angle between the reconstructed K_S^0 direction and the K_S^0 vertex direction from IP,
- z_dist: The z distance between two daughter tracks at their interception point,
- fl : The flight length of K_S candidate in x-y plane.

We optimize the parameters to maximize the $S/\sqrt{S+N}$. We use the K_S from 1000000 τ pair with generic decay Monte Carlo as samples and identify true K_S with the information from generator. Figure 4.1 shows the invariant mass, momentum and angular distribution of the samples. Figure 4.2 shows the distribution of each parameters and Figure 4.3 shows the plots of $S/\sqrt{S+N}$. According to these plots, we set the cut values of these parameters.

In addition, we reject Vee event with daughter particle s with electron ID (see next sub-section). Also, we reject Vee event with large $M(e^+e^-)$ where $M(e^+e^-)$ is the invariant mass assuming electron mass for the daughter tracks, in order to reject the background from the process of $\gamma \to e^+e^-$.

Figure 4.5 shows the invariant mass distribution after passing the K_S cuts. We fit double Gaussian for signal peak and liner function for background. The peak appeared in Monte Carlo is narrower. The background level of Monte Carlo is lower than that of the data. As shown in the Table 4.1, the number of the events are consistent within the 10% between data and Monte Carlo. The mean value of all Gaussian functions are consistent with the K^0 invariant mass value of world average. [23]

Finally, we set signal window of invariant mass as the 3σ of Gaussian fit for data. We confirm the quality of selected K_S^0 sample by using the life time of K_S candidate. We observe flight length fl^*, momentum p and invariant mass M of K_S candidate and calculate event by event lift time t:

$$t = \frac{fl^*}{p/M}. \tag{4.1}$$

Figure ?? shows the distributions of t for data. We obtain mean life time $c\tau$ from

Table 4.1: Fit results of K_S invariant mass after selections.

	Data	Monte Carlo
Signal yield	137502±371	126251±355
Background	29016±170	26017±161
Fitting parameters		
wide Gaussian		
constant	3577±146	3945±181
mean value (MeV/c^2)	497.91±0.04	498.03±0.03
sigma (MeV/c^2)	5.213±0.084	4.278±0.07
narrow Gaussian		
constant	17243±142	19361±168
mean value (MeV/c^2)	497.67±0.01	497.83±0.01
sigma (MeV/c^2)	2.099±0.018	1.729±0.017
liner function		
slope	-2167±205	-1155±188
constant	1605±102	1048±93

the slope of fitting of exponential function to these distributions. $c\tau = 2.35 \pm 0.01$, are consistent with the world average 2.68 ± 0.00 [23].
K_S cut values are summarized below.

- $d\phi < 10°$
- $z\_dist < 1.0$ cm
- $fl > 0.2$ cm
- $eid.prob(daughters) < 0.1$
- $M(e^+e^-) > 0.2$ GeV/c^2
- 0.490 GeV/$c^2 < M(\pi^+\pi^-) < 0.505$ GeV/c^2

4.2.4 Lepton identification

On the signal side of the topology, the remaining track is required to satisfy either electron or muon identification criteria.

- electron identification: $eid.prob() > 0.9$,
- muon identification: $muid.likelihood() > 0.9$.

Electrons are identified by requiring that the ratio of the energy deposited by the particle in the ELC to the momentum measured in the CDC is close to unity, and by using dE/dx information from the CDC and hits in the ACC.
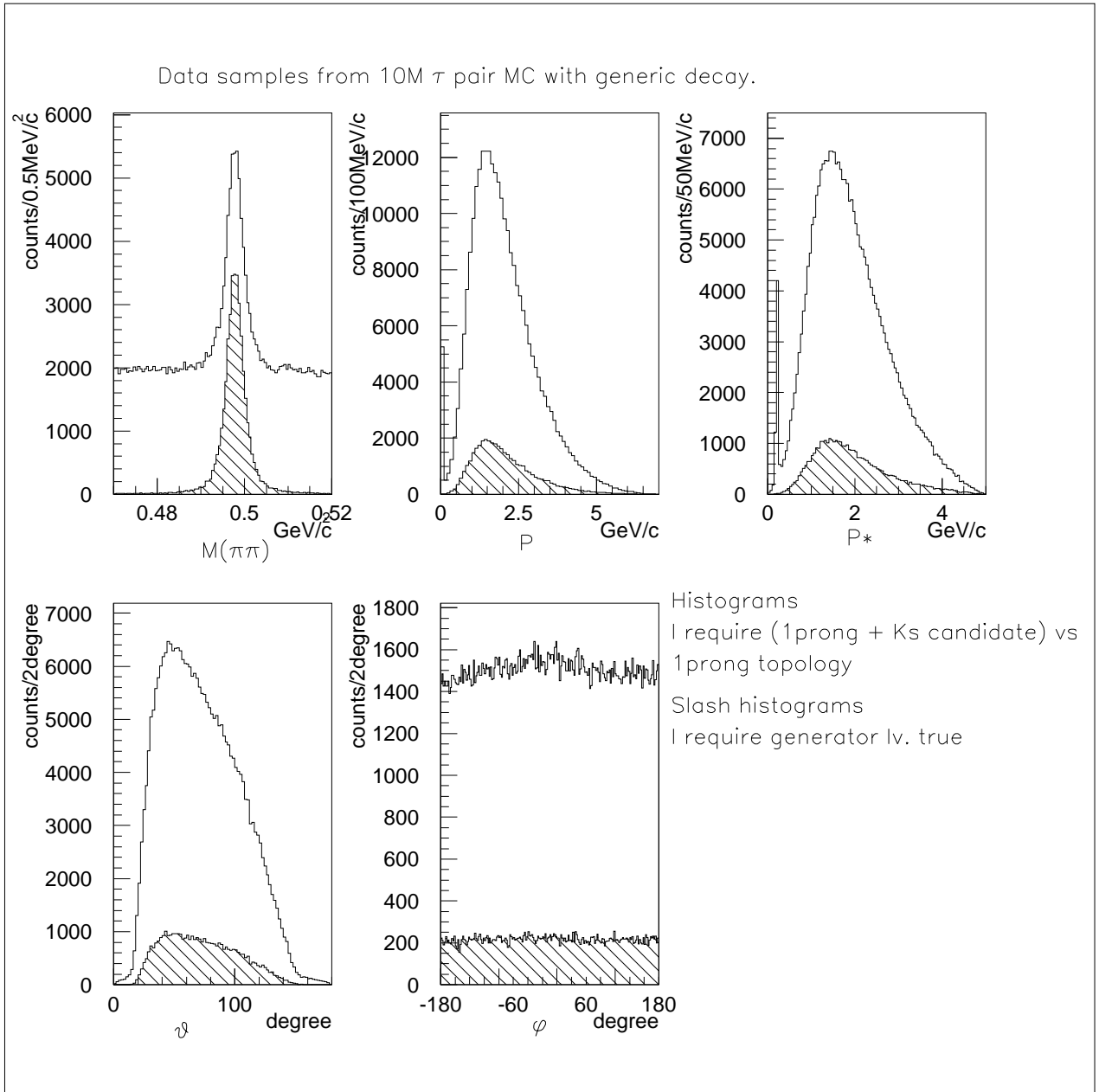
28

Figure 4.1: K_S sample from 10M τ pair events. We used this sample to optimize the cut parameters. Open hists are all sample, shaded are true in generator information.
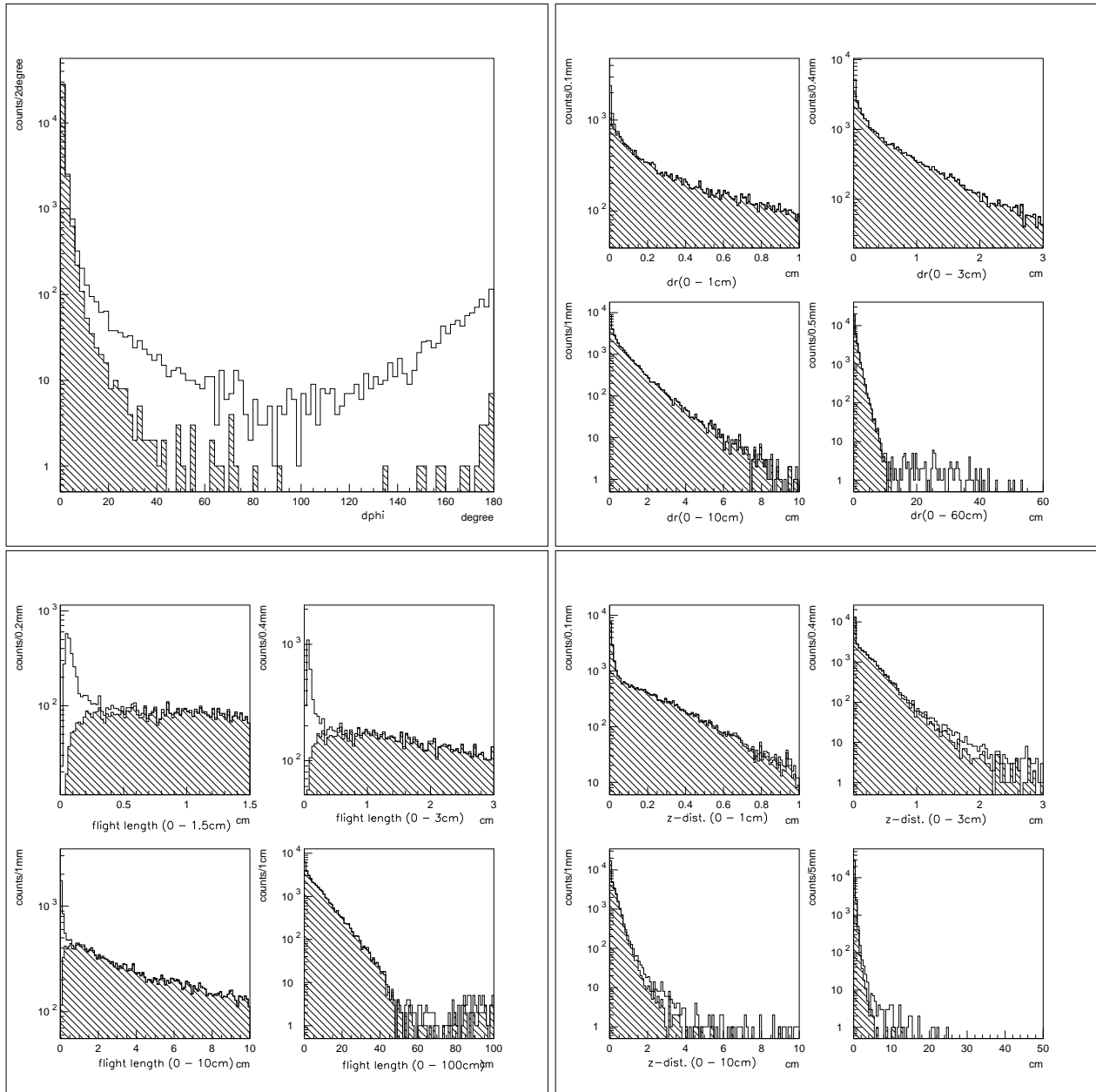
Figure 4.2: K_S cut Parameter distributions. Open hists are all sample, shaded are true in generator information.
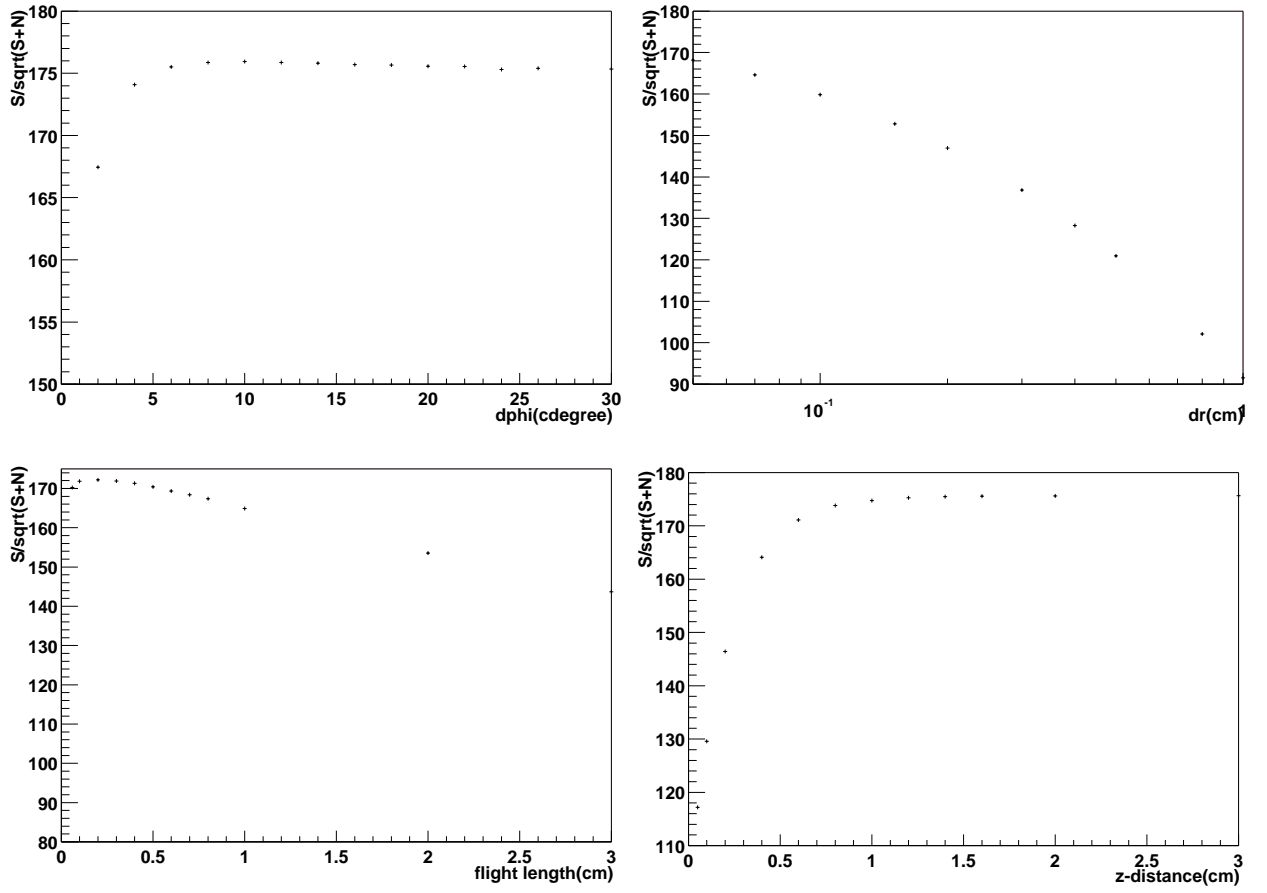
Figure 4.3: S/N ratio of K_S cut Parameters.

hall_ks

Nent = 168996

Mean = 0.4975

RMS = 0.007291

Chi2 / ndf = 251 / 47

Constant1 = 1.724e+04± 141.8

Mean_value1 = 0.4977± 1.028e-05

Sigma1 = -0.002099± 1.804e-05

Constant2 = 3577± 145.7

Mean_value2 = 0.4979± 3.831e-05

Sigma2 = 0.005213± 8.441e-05

Slope = -2167± 205.2

Constant3 = 1605± 102.5

hallmc_ks

Nent = 154677

Mean = 0.4977

RMS = 0.006968

Chi2 / ndf = 402.8 / 47

Constant1 = 1.936e+04± 168.2

Mean_value1 = 0.4978± 8.735e-06

Sigma1 = -0.001729± 1.649e-05

Constant2 = 3945± 180.5

Mean_value2 = 0.498± 3.125e-05

Sigma2 = 0.004278± 7.462e-05

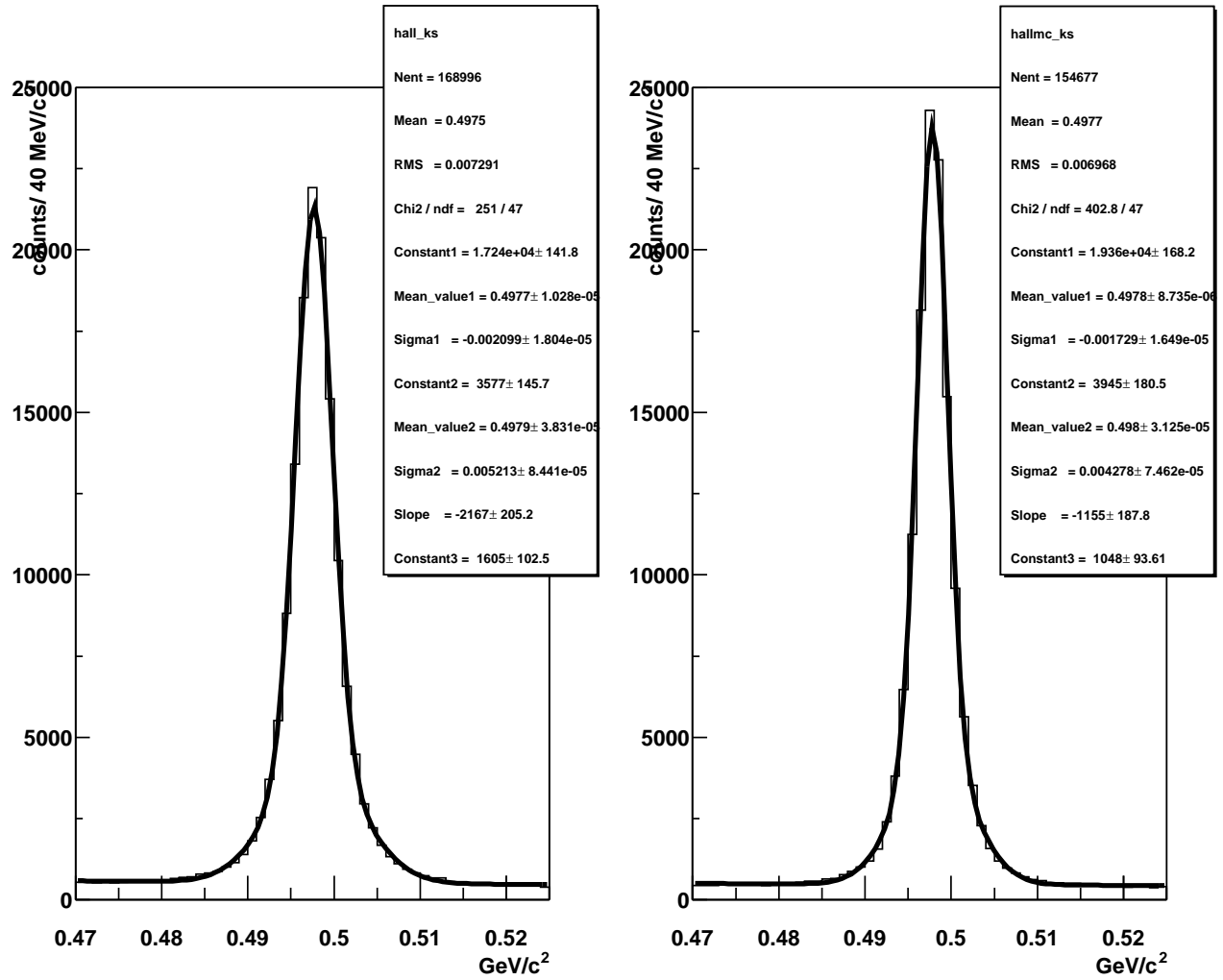Slope = -1155± 187.8

Constant3 = 1048± 93.61

Figure 4.4: The $M(\pi\pi)$ distributions of data and Monte Carlo normalized to the data using integrated luminosity.
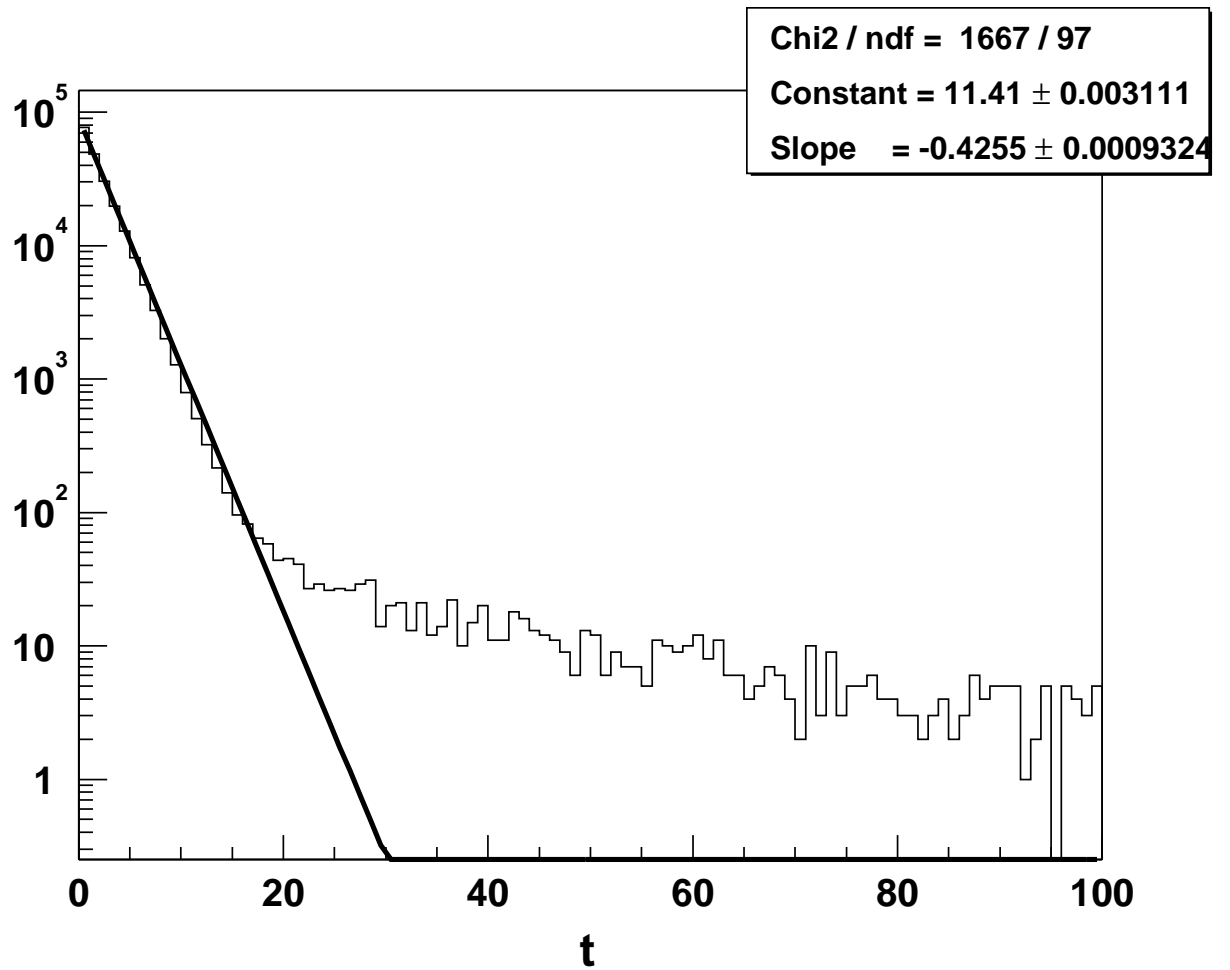
Figure 4.5: The $t(= \frac{fl^*}{p/M})$ distributions.

We estimate single electron ID efficiency using electrons embedded onto Hadronic data and generic Monte Carlo. The generic Monte Carlo consists of $B\bar{B}$ and $q\bar{q}$ with the ration of 1:3. We also estimete fake rate for pion using pion sample measured in K_S in hadronic event. The results are summarized in Figure 4.6. As shown in Figure 4.7, the momentum of electrons from signal decay are larger than 1 GeV/c at barrel region and 1.5 GeV/c at endcap region in the laboratory frame. We estimate efficiency is larger than 90% at barrel region and 85% at endcap region and fake rate for pion is 0.2% in whole region.

Muon candidates are required to have a well reconstructed track in the muon system comprised of 14 layers of iron plate interleaved with KLM. Muon probability is calculated from two variables; one is the difference between the range calculated by the momentum of the particle and the range measured by KLM, and the other is the chi-square of the KLM hits with respect to the extrapolated track.

We estimate efficiency and fake rate using muons from two photon process and charged pion from K_S decay, respectively. Figure 4.8 shows the momentum dependance of efficiendy and fake rate. The effciency is larger than 80% and fake rate is smaller than 2% in the momentum region of leptons from the decay of $\tau \to \ell \ K^0$. We do not require any particle identification for the charged track on the 1-prong side.

The detail and genaral description of electron and muon identification system in the Belle is summarized in Ref. [24][25].

4.2.5   Kinematics

In the QED process of τ pair production from the $e^+ e^-$ collision, photon radiation is attend with some probabilities, so that energy is lost from the system (initial state radiation). The radiation of photon is occured from electrons. If the tracks satisfy the loose electron identification condition: $eid.prob() > 0.5$, we correct the energy of electron by adding the photon energy less than 1.0 GeV, where photons are within the 10 degree cone around the track direction. Figure 4.9 shows the total energy distributions of signal Monte Calro before and after energy correction for electrons. A narrow peak of signal events is seen at 5.29 GeV, the beam energy E^*_{beam} in the CM system. Figure 4.10 shows the total energy distributions of data and Monte Carlo in CM system after application of criteria described above. These distributions also have been corrected with photon radiation energy from electron. The generic decays of τ and semi-leptonic decays of D meson are main backgrounds. The peaks are well separated from these background. We require the energy difference

$$\Delta E^* = E^* - E^*_{beam} \tag{4.2}$$

in the $e^+ e^-$ CM system to be consistent with zero:

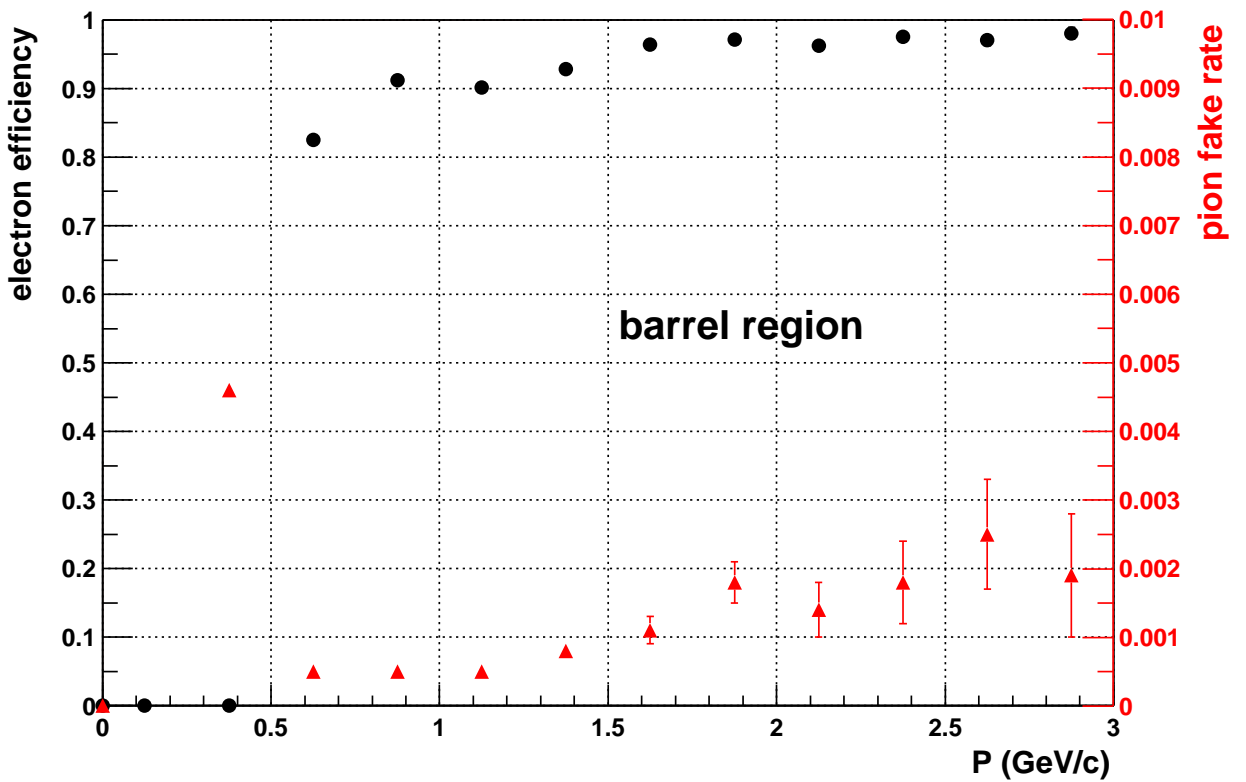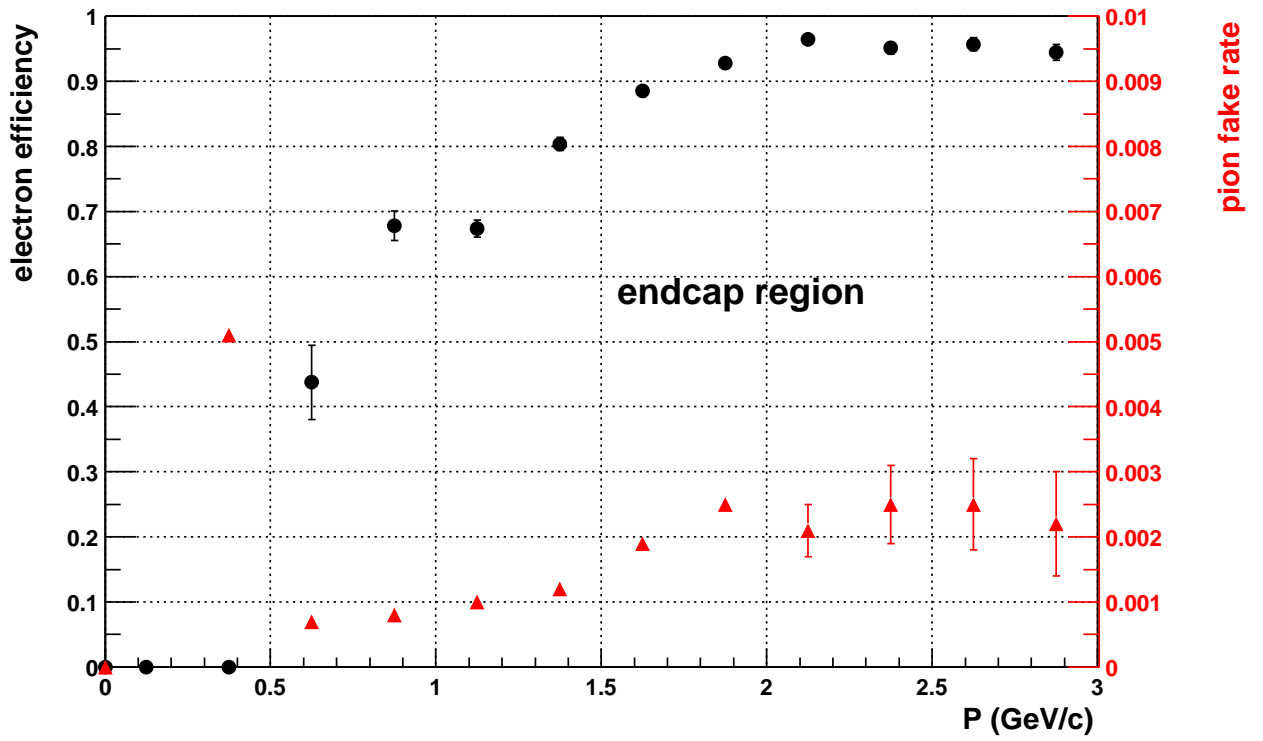- -0.49 GeV $< \Delta E^* <$ 0.01 GeV for $\tau \to e \ K^0$

34

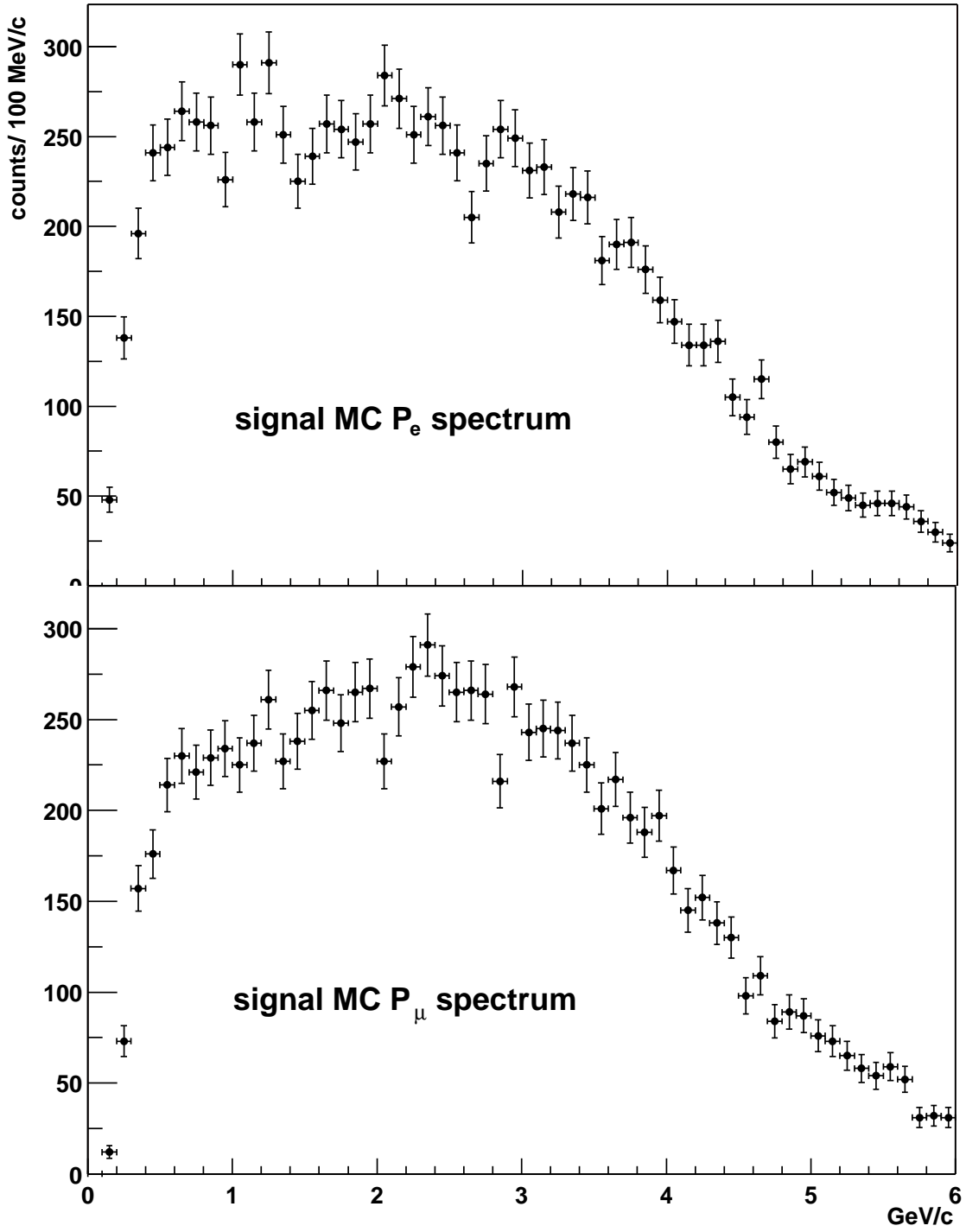Figure 4.6: The momentum dedendence of efficiency and pion fake rate of electron identification.

Figure 4.7: The momentum spectrum of leptons from the decay of $\tau \rightarrow \ell \ K^0$ processes.
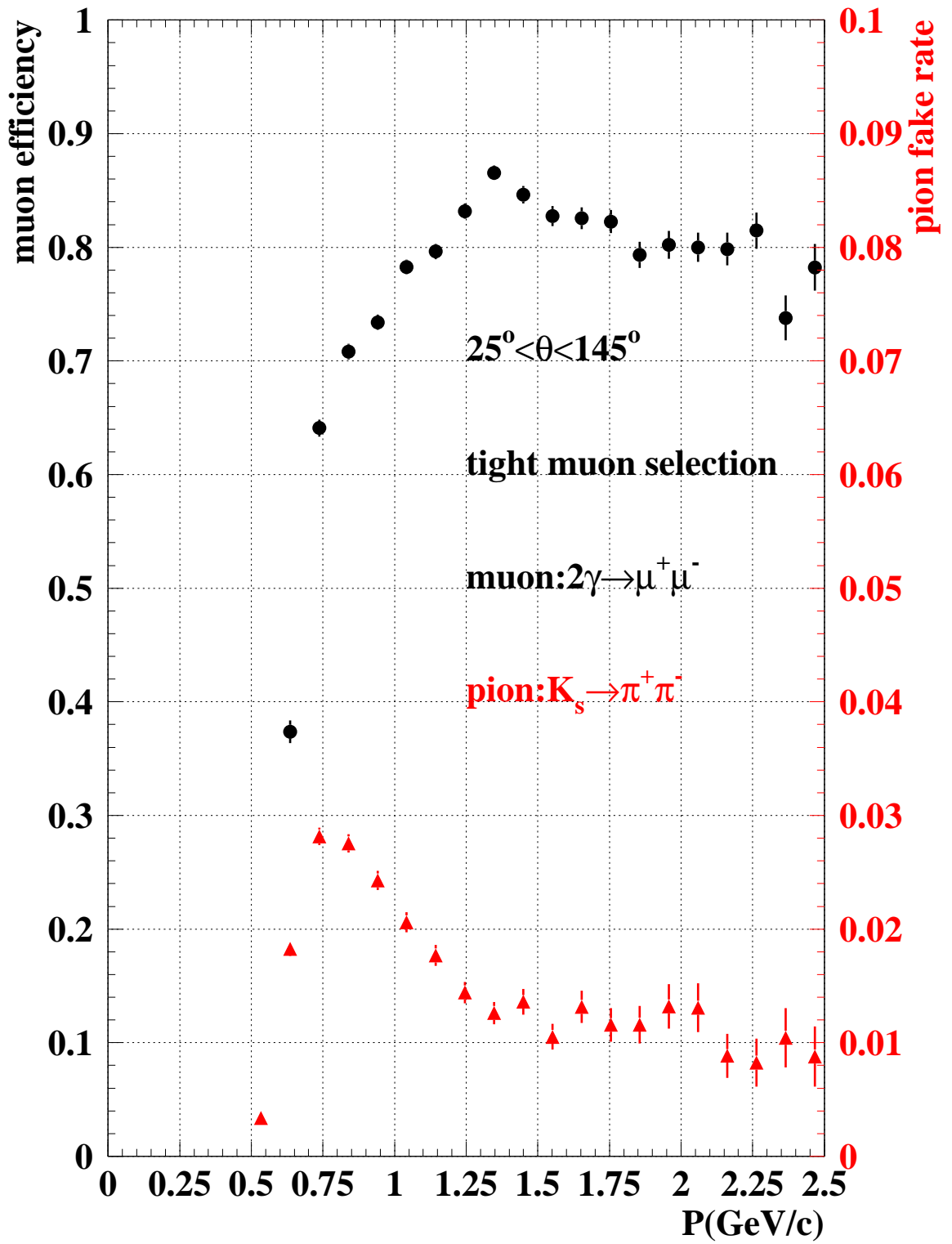
Figure 4.8: The momentum dedendence of efficiency and pion fake rate of muon identification.

- -0.29 GeV $< \Delta E^* < 0.01$ GeV for $\tau \to \mu\ K^0$.

For the signal candidates passing the all criteria , the invariant-mass $M(\ell\ K^0_S)$ distributions of the $(e\ K^0)$ and $(\mu\ K^0)$ systems on the 3-prong side are examined. Figure 4.11 shows the $M(\ell\ K^0_S)$ distributions after cuts (i)~(iv) for (a) $\tau \to e\ K^0$ (MC), (b) $\tau \to \mu\ K^0$ (MC), (c) $e\ K^0_S$ and (d) $\mu\ K^0_S$ for the data and MC backgrounds. The mass resolution from the signal MC simulation is due to the Belle detector performance. The standard deviation for a Gaussian fit to the mass distribution from the signal MC is found to be 9 MeV/c^2 for $(e\ K^0)$ and 8 MeV/c^2 for $(\mu\ K^0)$. We require the invariant mass of $\ell\ K^0$ system on the signal side to be in the 3σ region of the Gaussian fit around the invariant mass of τ ($= 1.777$ GeV/c^2):

- 1.752 GeV/$c^2 < M_{\ell\ K^0} < 1.802$ GeV/c^2

4.3 Results

The results when we process the Monte Carlo and the data under the condition we set in previous section are given.

4.3.1 Signal reconstruction efficiency

We estimate how many the signal events are reconstructed by counting the signal Monte Carlo events after processing with our analysis method. The two columns of "$e\ K^0$" and "$\mu\ K^0$" in Table 4.2 show the result at each selection step for the signal Monte Carlo. From these numbers, we expect the reconstruction efficiency ϵ to be:

$$\epsilon(e\ K^0) = 4.87 \pm 0.07\%$$
$$\epsilon(\mu\ K^0) = 4.78 \pm 0.07\%,$$

including branching fractions of K^0 decay, $K^0 \to K^0_S \to \pi^+\pi^-$. The errors quote only the statistics of Monte Carlo.

4.3.2 Experimental data

We processed all available data taken by Belle detector from January 2000 to July 2001. Figure 4.11 shows the invariant mass plot after lepton identification and total energy cut.

$\tau \to e\ K^0$ and $\tau \to \mu\ K^0$ show almost same distribution eccept for the appearence of the peak around $M(\ell\ K^0) \sim 0.9$ GeV/c^2 in the $\mu\ K^0$ mass distribution. This peak consists of $K^*(892)^\pm \to K^0\pi^\pm$ from generic τ decay and appeared only when
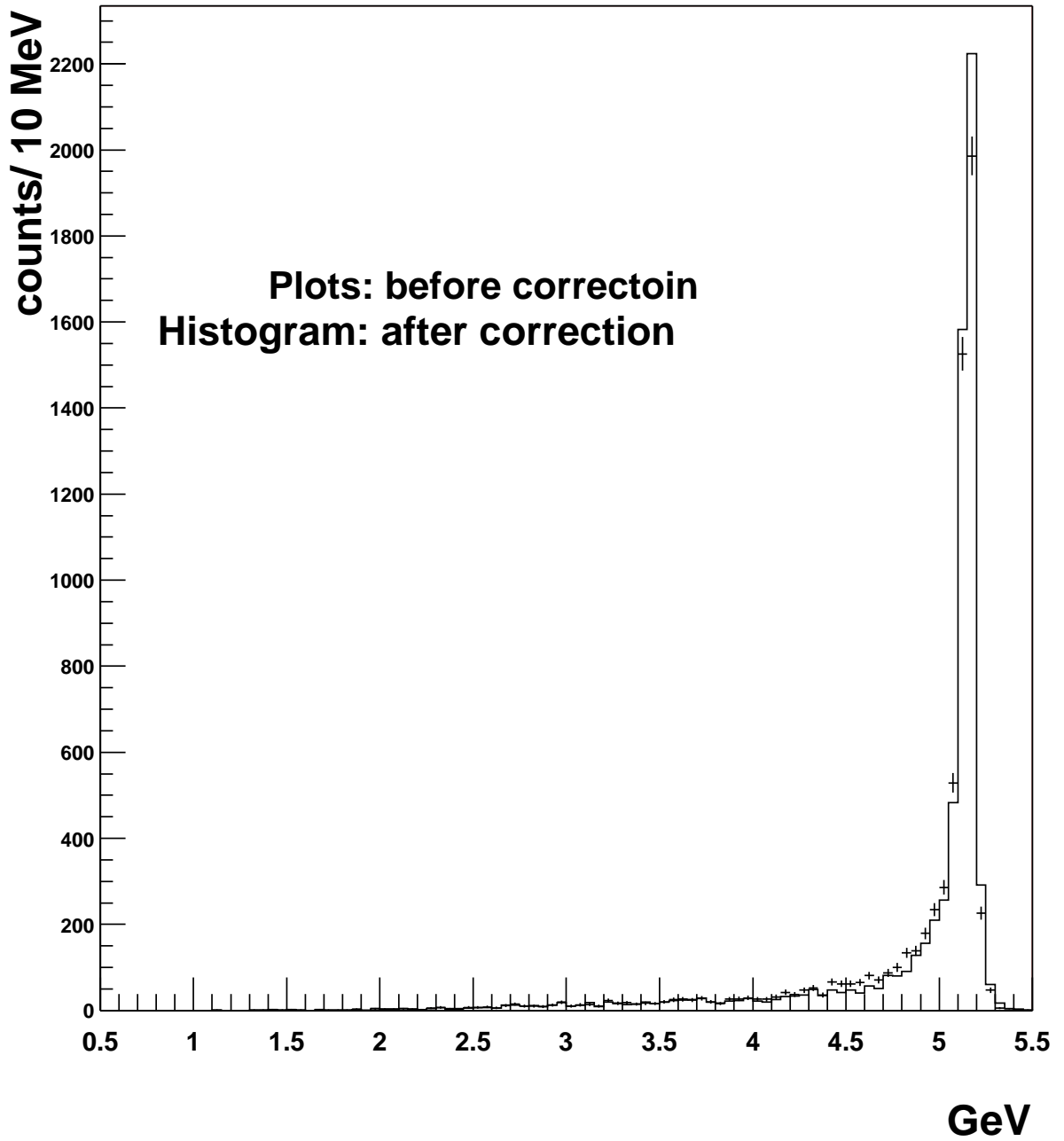
38

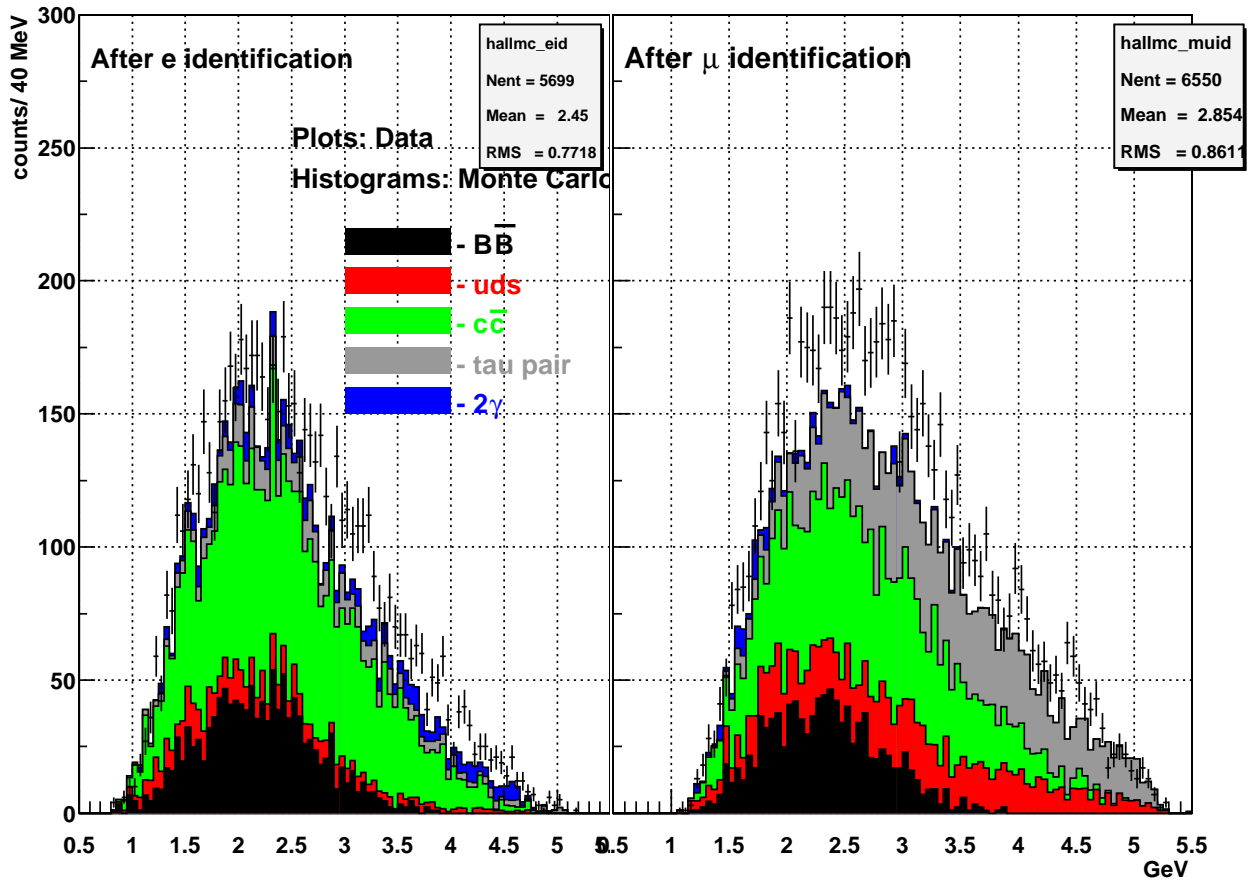Figure 4.9: E* distribution of signal MC before/after electron energy correction.

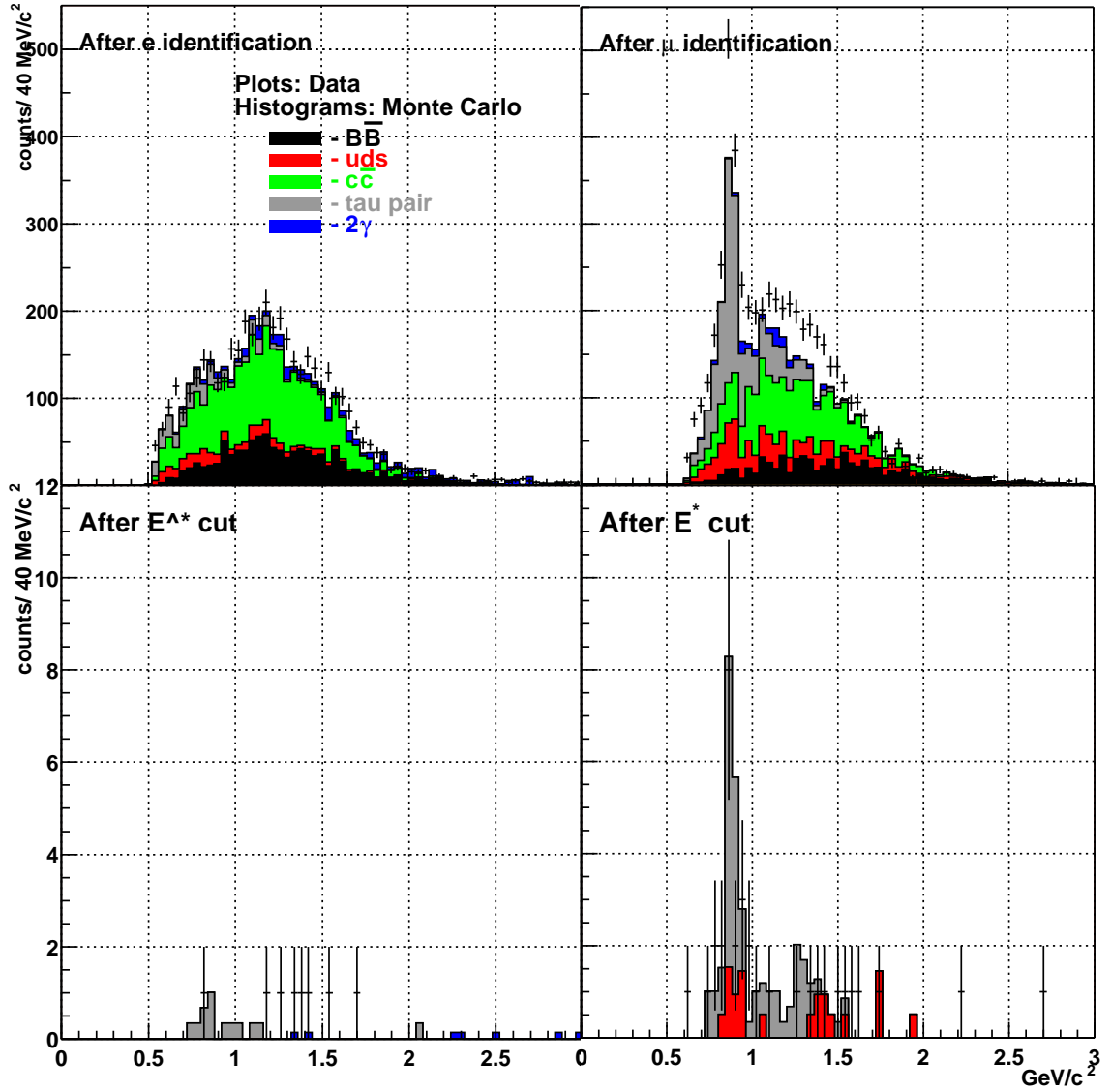Figure 4.10: The $E^*(\ell\ K_S)$ distributions.

40

Figure 4.11: The $M(\ell\ K_S)$ distributions.

41

we required $muid.likulihood()$ because the muon fake rate for pion is 10 times larger than that of electrons.

There are no signal candidates in the signal window after all cuts. We checked for all events satisfying the selection criteria with the wider signal region as 1.7 GeV/$c^2 < M(\ell\ K^0) < 1.85$ GeV/c^2. We define additional tighter criteria that the signal event might be satisfied:

- ΣE_γ is consistent to be 0 when the particle of 1-prong side is lepton.
- $(m_\nu)^2$ is consistent to be 0 when the particle of 1-prong side is hadron.
- E_ν^* is consistent to be not 0.
- θ_{miss} is in barrel region.

where

- $\cdot$ m_ν: the missing mass
- $\cdot$ E_ν^*: the missing energy in the CM system of e^+e^-
- $\cdot$ θ_{miss}: the direction of missing momentum

No events survive even if we set the invariant mass window wider. We consider no signals are observed in the data sample. To estimate backgounds in the signal window, we try to fit with the multi-order polynominal function to the invariant mass distributions of the data after all cuts except for mass cut. The background is consistent to be zero within the error of fitting parameters.

4.3.3 Background estimation

We checked how many background events will appear on and around our signal window. The numbers of events after passing the each cuts are summarized in Table 4.2. Figure 4.11 shows the invariant mass plot for Monte Carlo background normalized to data using luminosity after lepton identification and total energy cut. There is an excess of experimental data over Monte Carlo, especially in $M(\mu\ K^0) > 1.0$ GeV/c^2 region. According to the distribution on each selection steps we consider this difference mainly consists of decays of D meson from $c\bar{c}$ background. We suspect the models of $c\bar{c}$ Monte Carlo cannot represent for data accurately. As mentioned in "Kinematics" subsection, background from D meson decay is supressed by ΔE^* cut. As shown in the bottom of distribution in Figure 4.11, most of the background from $c\bar{c}$ are rejected after the ΔE^* cut. We consider the effect from this discreapancy is very small in the final step.

The distribution is considered to consist of two component. The peaks appear around $M \sim 0.9$ GeV/c^2 region in the τ pair Monte Carlo. As mentioned at the previous secion, this peak is causes from the miss identification of the pion which come from $K^*(892)$ in $\tau \rightarrow K^*(892)\nu$ decays. There is almost no peak if we require the signal lepton as electron because the pion fake rate of electron identification

42

Selection step	$e^-\ K^0$	$\mu^-\ K^0$	$B\bar{B}$	uds	$c\bar{c}$	τ pair
Cross sction (nb)	—	—	1.05	2.09	1.30	0.91
Events normalized to data(10^6)	—	—	28.1	61.4	38.2	26.8
Analyzed events(10^6)	0.1	0.1	40.0	99.0	52.0	50.0
Event topology	10961	11361	64744	695294	286637	1332271
K_S^0 selection	7694	7938	6617	101400	50840	166801
Lepton ID	6749	6401	2005	2547	7403	4529
$E^*(\ell\ K^0)$	5481	5045	0	26	1	91
$M(\ell\ K^0)$	4873	4782	0	0	0	0

	$eeee$	$ee\mu\mu$	$eeuu$	$eess$	$eecc$	Data
Cross sction (nb)	40.9	18.9	11.7	0.23	0.03	—
Events normalized to data(10^6)	1200	556	344	6.76	0.88	—
Analyzed events(10^6)	100.0	100.0	100.0	50.0	1.0	29.4 fb^{-1}
Event topology	176	857	8679	16827	7505	988396
K_S^0 selection	0	6	902	6682	1232	138700
Lepton ID	0	4	45	1186	160	9657
$E^*(\ell\ K^0)$	0	0	0	10	0	44
$M(\ell\ K^0)$	0	0	0	0	0	0

Table 4.2: The number of events passing each criteria steps.

is ten times smaller than that of muon. This peak is distributed only around the region of 0.7 GeV/c^2 < M < 1 GeV/c^2, so there is no effect to our signal region. The other component has multi-order polynominal function shape and consists of random source from generic τ decay with low energy neutrinos, continuum event which contains fake lepton and so on. These events are well supressed by the selection criteria, but tail spreads to the signal region. We estimate the background level in the signal window by the same method as experimental data analysis. As same as the fitting to experimental data, each parameters of fitting functions are consistent with zero within the errors.

4.4   Systematic Errors

In this section, we test the efficiencies obtained from Monte Carlo control sample data. We assume that our Monte Carlo describes our detector well and only need a correction for experimental data. We correct our signal reconstruction efficiency by multiplying the correction factor f;

$$f = \frac{\epsilon_{data}^{tracking}}{\epsilon_{MC}^{tracking}} \times \frac{\epsilon_{data}^{K_S\ selection}}{\epsilon_{MC}^{K_S\ selection}} \times \frac{\epsilon_{data}^{e/\mu\ identification}}{\epsilon_{MC}^{e/\mu\ identification}} \tag{4.3}$$
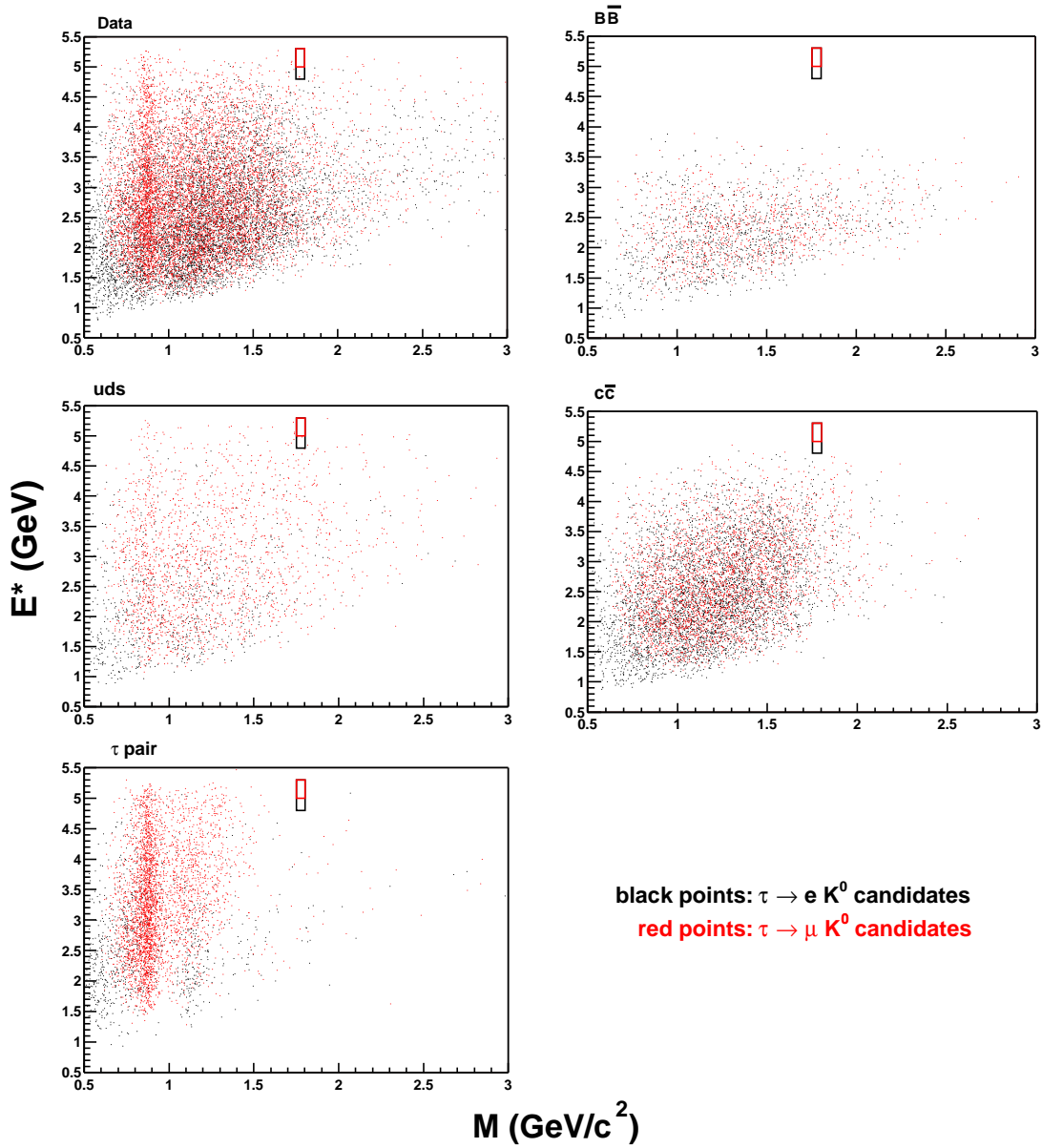
Figure 4.12: The $E^*(\ell\ K_S)$ vs $M(\ell\ K_S)$ distributions of data and Monte Carlo ($B\bar{B}, uds, c\bar{c}$, and τ pair) after passing the lepton identifications. Black points are identified as "electron" and red points are identified as "muon". The boxes show the signal windows: black for $\tau \to e\ K^0$ and red for $\tau \to \mu\ K^0$.
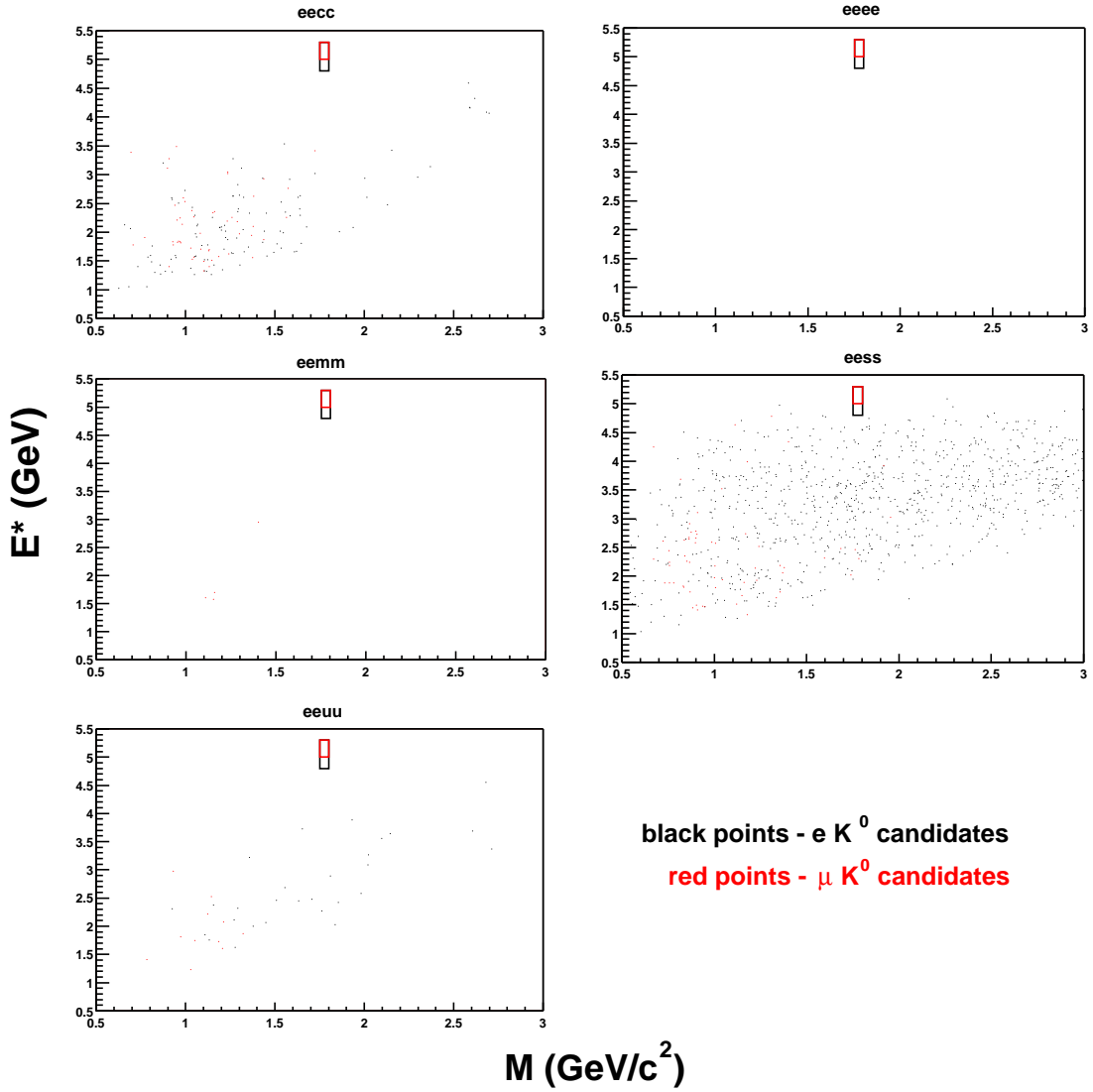
Figure 4.13: The $E^*(\ell\ K_S)$ vs $M(\ell\ K_S)$ distributions of two-photon process Monte Carlo. Black points are events identified as "electron" and red points are identified as "muon". The boxes shows the signal windows: black for $\tau \to e\ K^0$ and red for $\tau \to \mu\ K^0$.
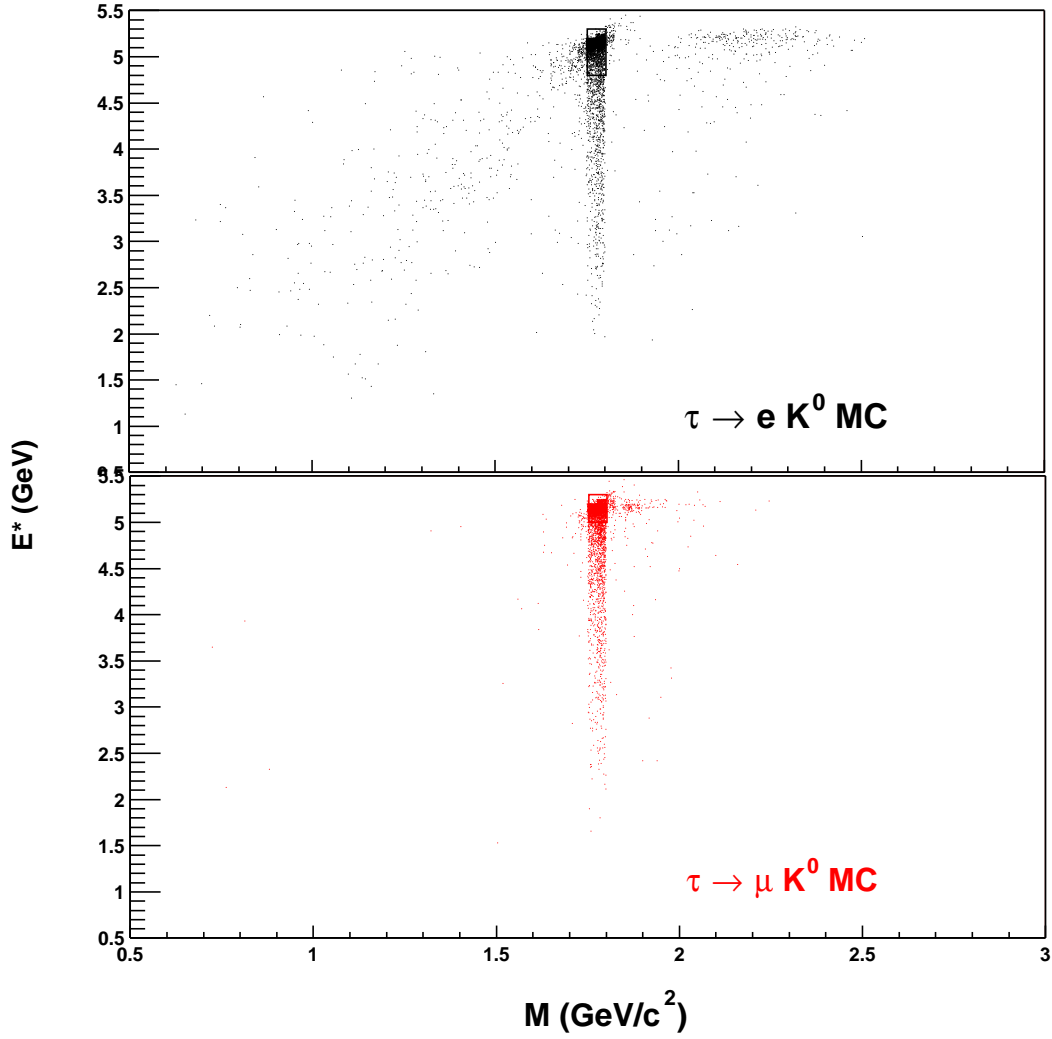
Figure 4.14: The $E^*(\ell\ K_S)$ vs $M(\ell\ K_S)$ distributions of each signal Monte Carlo after passing the lepton identifications. Top and bottom are $\tau \to eK^0$ and $\tau \to \mu K^0$, respectively. The boxes show the signal windows.

46

where ϵ is the reconstruction efficiency when adopting the criteria. We suppose that the associated errors are uncorrelated, and define the systematic error of the signal reconstruction efficiency as combination of the errors of each correction factors.

4.4.1 Tracking

The difference in tracking efficiencies between the experimental data and Monte Carlo has been studied by comparing the yield ratio

$$\epsilon(\pi^+\pi^-) = N(\eta \to \pi^+\pi^-\pi^0)/N(\eta \to \gamma\gamma). \tag{4.4}$$

where N denotes the number of signal yield.
By taking the ratio, we assume the systematic difference in the photon detection cancels out, and then obtain the relative efficiency for pion tracks. We quote the result of [26],: the analysis using full set of the experimental data and 30M continuum Monte Carlo sample:

$$\sqrt{\epsilon_{data}(\pi^+\pi^-)/\epsilon_{MC}(\pi^+\pi^-)} = 0.9824 \pm 0.0253.$$

A correction for the Monte Carlo generator is included and the error mainly comes from the fitting for signal yield. This quantity is interpreted as the difference of single track efficiency between the data and Monte Carlo. As we use two tracks of signal lepton and 1-prong side track in this analysis, the correction factor is

$$\frac{\epsilon_{data}^{tracking}}{\epsilon_{MC}^{tracking}} = 0.9652 \pm 0.0358.$$

4.5 K_S selection

We estimate the difference in K_S detection in the environment of our analysis between the experimental data and Monte Carlo by comparing the $M(\pi^+\pi^-)$ yield after K_S selection. We obtain:

$$\frac{\epsilon_{data}^{K_S \; selection}}{\epsilon_{MC}^{K_S \; selection}} = 1.089 \pm 0.004,$$

using the number listed on Table 4.1. This includes the tracking efficiency for Vee daughters.

4.5.1 Lepton identification

Electrons

We obtain the electron detection efficiency by comparing the $J/\psi(\to e^+e^-)X$ yield for the case that one or two electrons are tagged. We use the sample which passes the standard hadronic event selection in Belle and additional cut for rejecting the QED related backgrounds such as radiative Bhabha events. To model the signal shape, we first fit the $M(e^+e^-)$ distribution of double tagged events with a function so called "crystal-ball function" for the signal and exponential for the background. The same procedure is carried out for the sample of single-tagged events, and that of single-tagged events substructed by the double-tagged events. The difference between single and double tagged events ΔN is:

$$\Delta N_{tag} \propto 1 - \bar{\epsilon}^2(2\bar{\epsilon}(1-\bar{\epsilon})) \tag{4.5}$$

where $\bar{\epsilon}$ denotes inefficiency. We estimate the inefficiency to be $(6.2\pm1.4)\%$ from the analysis of the data and $(5.6\pm0.1)\%$ from Monte Carlo. These correspond to

$$\frac{\epsilon_{data}^{e\ identification}}{\epsilon_{MC}^{e\ identification}} = 0.995 \pm 0.015.$$

Muons

We estimate the muon detection efficiency under high track density conditions using the muons from the $J/\psi \to \mu\mu$ decay in $B\bar{B}$ events for the "real" muons. We also analyze a overlaying simulating single-track muon on a hadronic event taken from real data. In the former case, we claclate the efficiency from the difference of the yield between single tagged and double tagged as same as electron identification. We obtain the efficiency for the "real" muons is $90.1\pm1.1\%$. The measured efficiency for muons in the hybrid events is $88.7 \pm 0.3\%$. We obtain correction factor for Monte Carlo is:

$$\frac{\epsilon_{data}^{\mu\ identification}}{\epsilon_{MC}^{\mu\ identification}} = 1.016 \pm 0.013.$$

4.5.2 Summary of signal reconstruction efficiency correction

Combining these systematic errors, we obtain the overall correction factor for Monte Carlo signal efficiency:

$$f = 1.05 \pm 0.04 \ (\tau \to e \ K^0)$$
$$f = 1.07 \pm 0.04 \ (\tau \to \mu \ K^0).$$

48

Table 4.3: The summary of systematic errors.

	error(%)
tracking	$\pm 3.6\%$
K_S selection	$\pm 0.4\%$
electron identification	$\pm 1.5\%$
muon identification	$\pm 1.3\%$

After correction by factor f , the signal reconstruction efficiency is estimated:

$$\epsilon(\tau \rightarrow e\ K^0) = 5.11 \pm 0.07 \pm 0.18\%$$
$$\epsilon(\tau \rightarrow \mu\ K^0) = 5.11 \pm 0.07 \pm 0.19\%.$$

where the first error is statistical and the second error is systematic error.

Chapter 5

Conclusions

Our signal reconstruction efficiencies are obtained as

$$\epsilon(\tau \to e\ K^0) = 5.11 \pm 0.07 \pm 0.18\%,$$
$$\epsilon(\tau \to \mu\ K^0) = 5.11 \pm 0.07 \pm 0.19\%.$$

These efficiencies contain the branching fraction of $K^0 \to K^0_S \to \pi^+\pi^-$ and estimated with Monte Carlo and corrected for data. The number of τ pair events analyzed $N_{\tau\tau}$ are decided from the integrate luminosity and the cross section of τ pair creation in the $e^+e^- \to \tau^+\tau^-$ QED process at the beam constrained energy. This value is caluclated by Monte Carlo generator and contains 0.29% of relative error. The integrated luminosity is obtained from the number of Bhabha event and conversion factor. The number of barrel Bhabha event is calculated from the number of CsI trigger and prescale factor. We estiate statistical error as 0.05% from the number of barrel Bhabha event but have not estimate systematical error yet.

$$N_{\tau\tau} = \int L dt \times \sigma(e^+e^- \to \tau^+\tau^-) = (26.75 \pm 0.08) \times 10^6.$$

We observe no signal candidates. The estimated observable background level is consistent with zero by examining the beam constrained mass spectrum. Using the frequent method [23] for small observed sample, the upper limit of observed events N_{obs} are 2.44 events at 90% confidence level.

From these, the branching fractions for $\tau \to e/\mu\ K^0$ are calculated by the formula below,

$$Br(\tau \to e/\mu\ K^0) < \frac{N_{obs}}{2 \times N_{\tau\tau} \times \epsilon(\tau \to e/\mu\ K^0)}. \tag{5.1}$$

When we take the lowest detection efficiencies within errors the upper limits are:

$$Br(\tau \to e\ K^0) < 0.94 \times 10^{-6},$$
$$Br(\tau \to \mu\ K^0) < 0.94 \times 10^{-6}.$$

The limits obtained this analysis are approximately three order of magnitude lower than those obtained at Mark II.

Appendix A

Other lepton flavor violating τ decay modes

We search for other lepton flavor violating τ decay process. We can analyze these mode by the almost same method as the search for the $\tau \to \ell\, K^0$ processes. The upper bound of branching fractions are listed in Table 2.1 in Chapter 2. The list of the Model B is not completed because among the processes proceeding at the one-loop level only the $l \to l'\gamma$ processes have been found. There are some mode with larger or same order theoretical upper bounds than the experimental results. With much higher statistics than that of previous experiments, we will assure their results and might reach the new physics.

A.1   Data samples

For experimental data, we process the same data sample as the $\tau\ell\, K^0$ analysis. On the other hands for background study, we use 40 $\times 10^6$ generic $B\bar{B}$, 79 $\times 10^6$ generic uds (combination $u\bar{u}, d\bar{d}, s\bar{s}$ continuum), 39 $\times 10^6$ generic $c\bar{c}$, 50 $\times 10^6$ generic τ pair, each 100 $\times 10^6$ $ee \to eeee$, $ee \to ee\mu\mu$, $ee \to eeuu$, 50 $\times 10^6$ $ee \to eess$ and 1 $\times 10^6$ $ee \to eecc$ samples. They are large enough comparing to the data size of this analysis.

For each LFV decay modes, we generate 10000 Monte Carlo events with one τ decaying into lepton flavor violating process and the other τ decaying into a generic mode.

A.2   Event selection

We change the selection criteria for the $\tau \to \ell\, K^0$ analysis for this analysis. We mention only the changed points here.

A.2.1　Pre-selection

Absence of the K_S selection raise the background level higher. We optimize the pre-selection criteria by data and signal Monte Carlo analysis. To suppress the radiative Bhabha or radiative mu-pair process, we require the total energy of photons in each event is smaller than 1 GeV. Also, we tighted the threshold of the total perpendicular momentum cut from 0.2 GeV/c to 0.5 GeV/c. Especially the four modes listed below are so noisy that we set the threshold as 1.0 GeV/c,

$$\tau^- \to e^- e^+ e^-, \tau^- \to e^- K^+ K^-, \tau^- \to \mu^- K^+ K^-, \tau^- \to \mu^- \rho^0.$$

A.2.2　Topological cuts

We change the requirement on event topology from "(1-prong + 1-Vee) vs 1-prong" to "3-prong vs 1-prong". The topology was defined by counting the number of tracks on plane perpendicular to the the thrust axis calculated from all charged tracks.

A.2.3　Particle identification

Some of the mode contains charged kaons and pions in the final state so we are required to identify them. As mentioned Chapter 3, Belle detector has good PID system as shown in Figure A.1. For every charged tracks, likelihood from ACC, TOF and CDC dE/dx are calculated with pion and kaon hypothesis. A combined likelihood is constructed for each hypothesis in such a way that a pion-like track gives zero and a kaon-like track gives one. We give a general name to this atc_pid. The detail of atc_pid system is described in Ref. [28]. We apply the following K/π separation cut:

$$atc\_pid(K/\pi) > 0.6 \text{ for kaons}$$
$$atc\_pid(K/\pi) < 0.4 \text{ for pions.}$$

The kaon selection efficiency for experimental data is typically 85% while the pion selection efficiency is 90%. In addion, we apply the cut for the pion as "not lepton":

$$eid.prob() < 0.01$$
$$muid.likelihood() < 0.1.$$

For lepton identifications, we require as same as $\tau \to \ell \ K^0$ analysis. The four momentum of each track is given according to its particles.
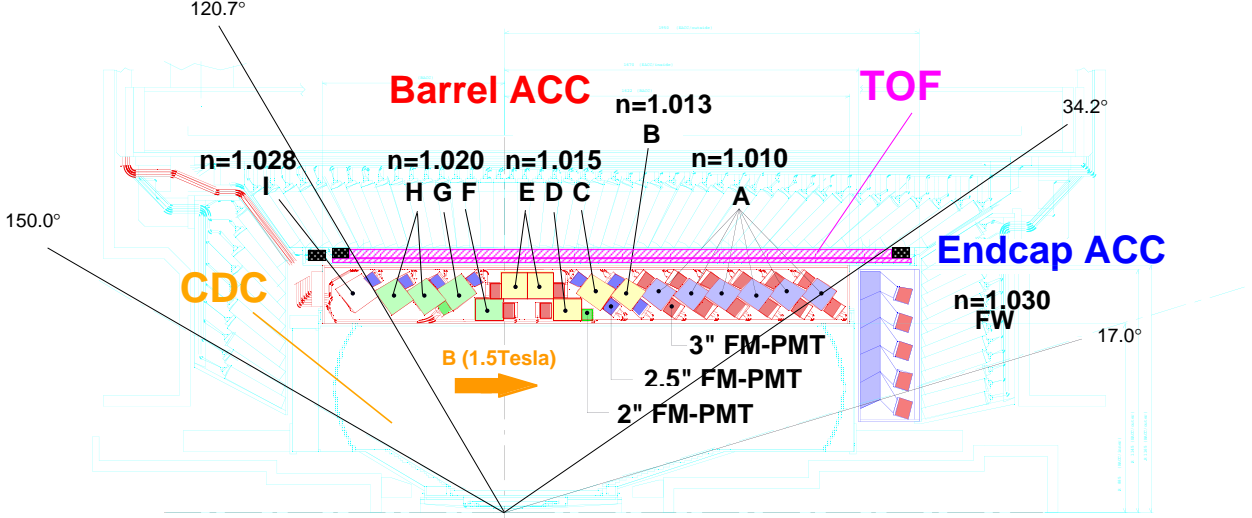
Figure A.1: The sideview of the Belle PID system.

A.2.4   Kinematics

After particle identification, We calculate total energy E^* and invariant mass M for 3-prong system in the CM of e^+e^-. We set signal selection cut from the study of background and signal Monte Carlo:

- -0.09 GeV $< \Delta E^* < 0.01$ GeV and

- 1.732 GeV/$c^2 < M < 1.812$ GeV/c^2.

For the process of $\tau \to \ell M^0$ (M^0 denotes a neutral meson), we require the invariant mass of M^0 reconstructed from two hadrons system is consist with each M^0 mass:

- 0.65 GeV/$c^2 < M(\pi\pi) < 0.90$ GeV/c^2 for ρ,

- 0.77 GeV/$c^2 < M(\pi K) < 1.01$ GeV/c^2 for $K^*(892)^0$ and

- 1.01 GeV/$c^2 < M(KK) < 1.03$ GeV/c^2 for ϕ.

When we analyze the process of $\tau \to \ell hh$ (h denotes a charged hadron), we require to exclude the M^0 invariant mass regions.
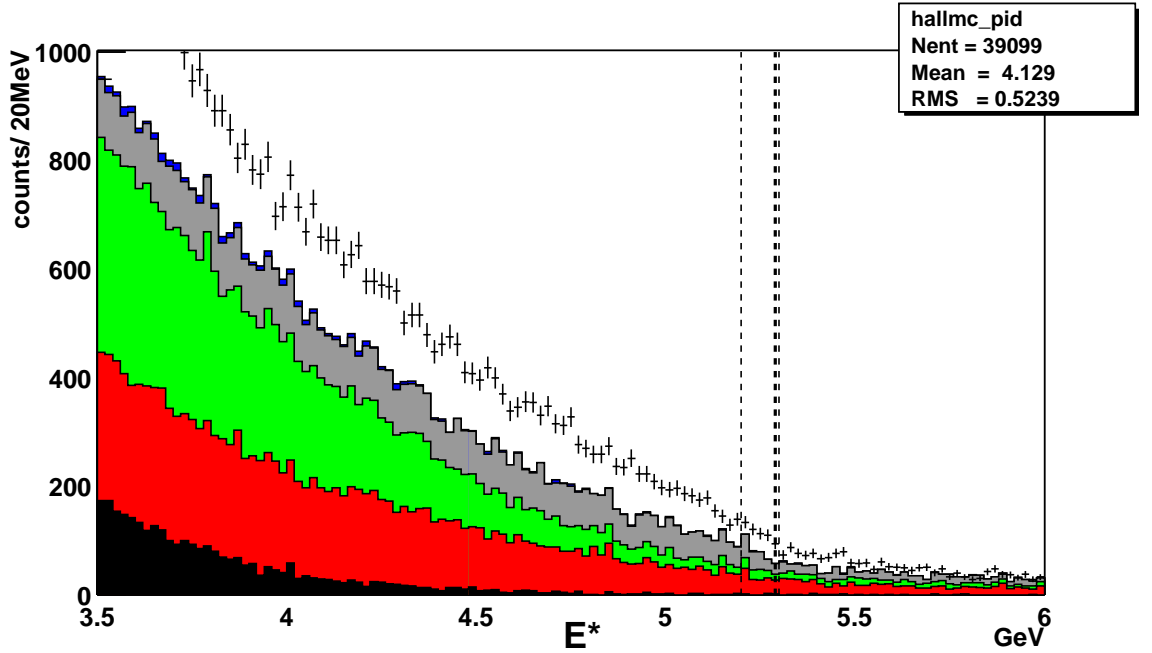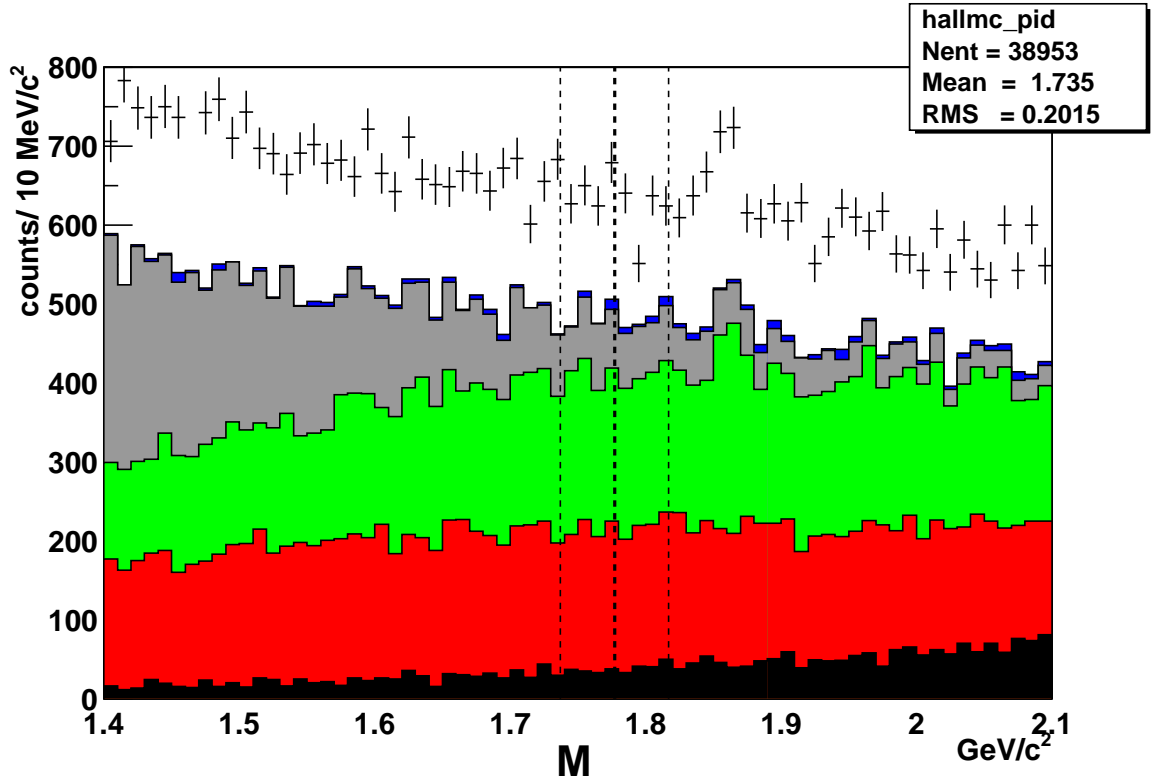
Figure A.2: The M and E^* distributions of data and Monte Carlo for all modes. Plots are data and histgrams are Monte Carlo: $B\bar{B}$(black), uds continuum(red), $c\bar{c}$ continuum(green), τ pair(gray) and 2 photon processes(blue).

55

Process	efficiency (%)	Exppected	Observed	U.L. ($\times 10^{-6}$)
$\tau \to e^- e^+ e^-$	5.9	2.0	8	3.6
$\tau \to \mu^- \mu^+ \mu^-$	5.5	1.3	1	1.1
$\tau \to e^- \mu^+ \mu^-$	5.9	0.7	3	2.1
$\tau \to \mu^- e^+ e^-$	6.2	0	4	2.6
$\tau \to e^+ \mu^- \mu^-$	6.0	0	0	0.76
$\tau \to \mu^+ e^- e^-$	7.4	0	1	1.1
$\tau \to e^- \pi^+ \pi^-$	7.4	2.5	6	2.3
$\tau \to \mu^- \pi^+ \pi^-$	6.5	5.9	11	3.4
$\tau \to e^- \pi^+ K^-$	8.2	0	2	1.3
$\tau \to \mu^- \pi^+ K^-$	6.1	1.3	3	1.9
$\tau \to e^- \pi^- K^+$	6.0	1.3	2	1.5
$\tau \to \mu^- \pi^- K^+$	5.5	2.0	2	1.3
$\tau \to e^- K^- K^+$	6.3	10.5	8	1.2
$\tau \to \mu^- K^- K^+$	5.5	10.6	12	2.9
$\tau \to e^- \rho^0$	7.0	3.2	5	1.8
$\tau \to \mu^- \rho^0$	6.9	8.6	11	2.5
$\tau \to e^- K^*(892)^0$	5.5	0	0	0.83
$\tau \to \mu^- K^*(892)^0$	4.9	0	0	0.93
$\tau \to e^- \bar{K}^*(892)^0$	5.4	0	2	2.0
$\tau \to \mu^- \bar{K}^*(892)^0$	5.2	1.3	4	2.6
$\tau \to e^- \phi$	4.2	0.7	2	2.3
$\tau \to \mu^- \phi$	3.3	0	5	5.6

Table A.1: The summarized results of the $\tau \to 3charged$ lepton flavor violating processes analysis.

A.3 Results and Summary

Figure A.2 shows all modes additional E^* and M distributions of data and Monte Carlo for all modes. There is no characteristic structures appeared significantly at τ mass (=1.777 GeV/c^2) anf E^* (5.29 GeV). Each of the data and Monte Carlo, there are few events in the signal windows after passing all cuts for some of the modes. We estimate signal reconstruction efficiencies from the analysis of each signal Monte Carlo. We obtain the upper end of observable events from the Poisson limits for small samples observed event from data and expected background from Monte Carlo. Using these, we set the upper limits for each lepton flavor violating modes by following with the equation (5,1). These results are summarized in Table A.1. These experimental limits are close to the allowed ranges of neutlinoless τ decay rates, predicted from models with heavy neutral leptons and right-left symmetries [3].
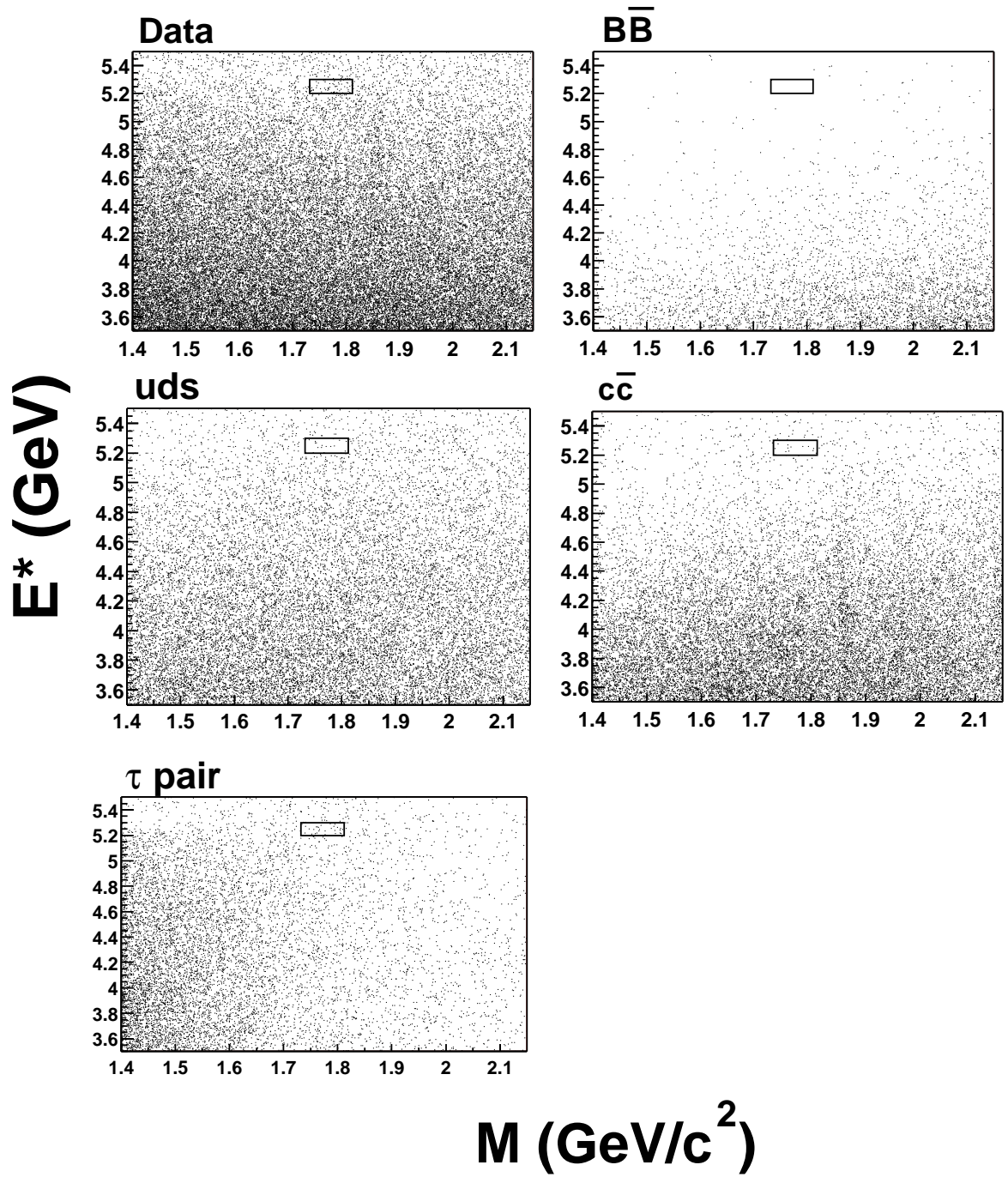
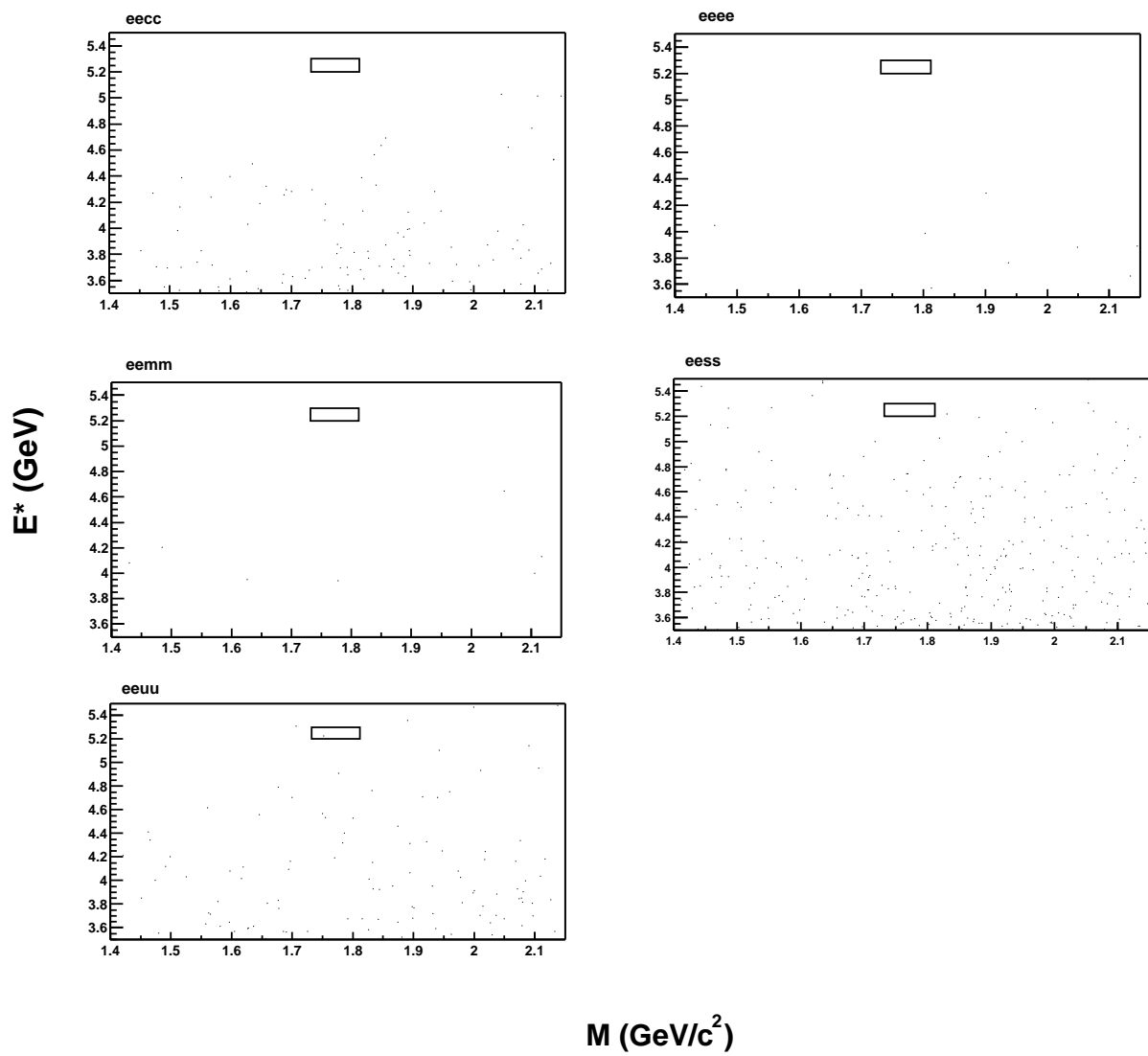Figure A.3: E^* vs M distributions of data and Monte Carlo.

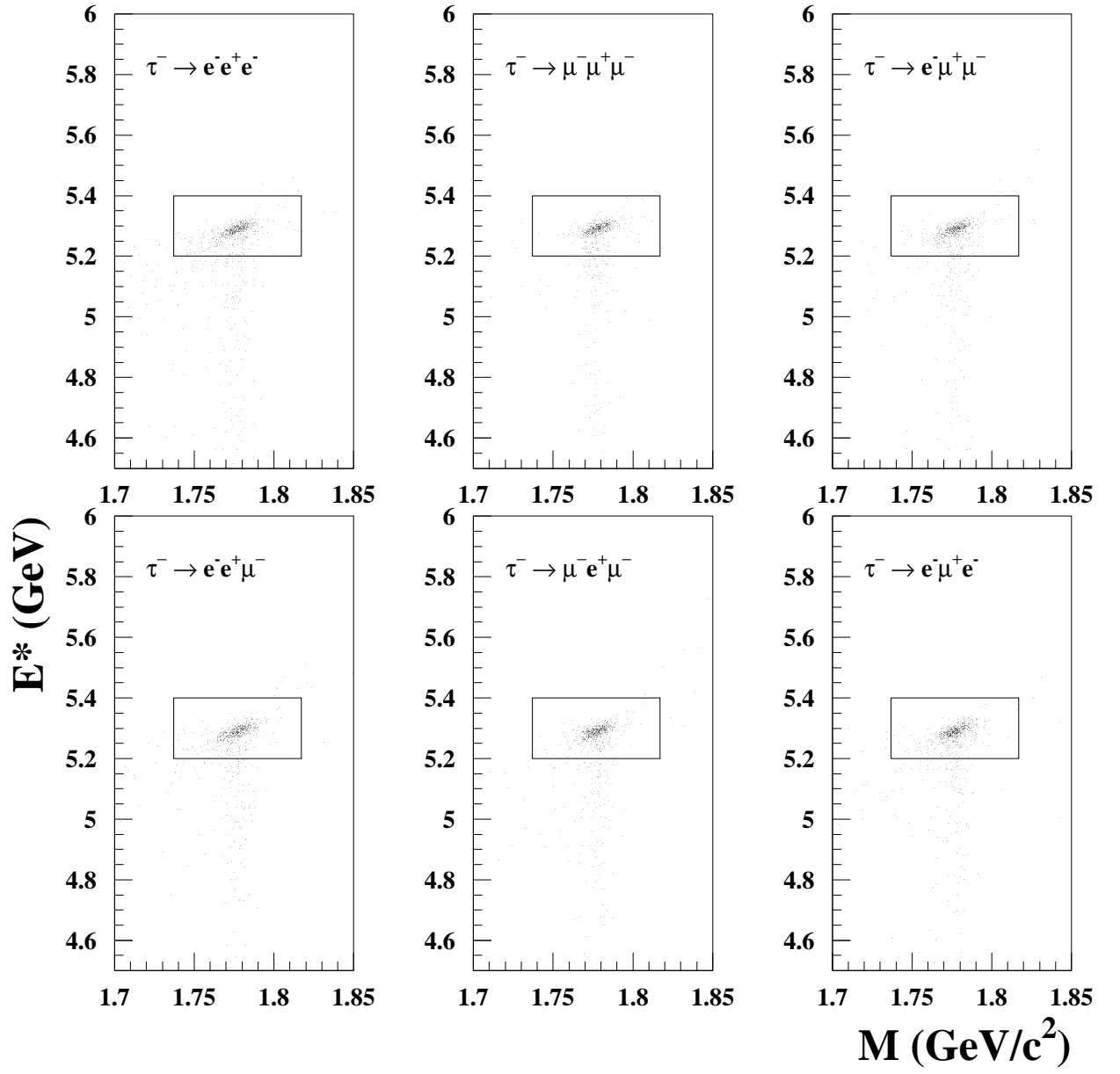Figure A.4: E^* vs M distributions of two photon process Monte Carlo.

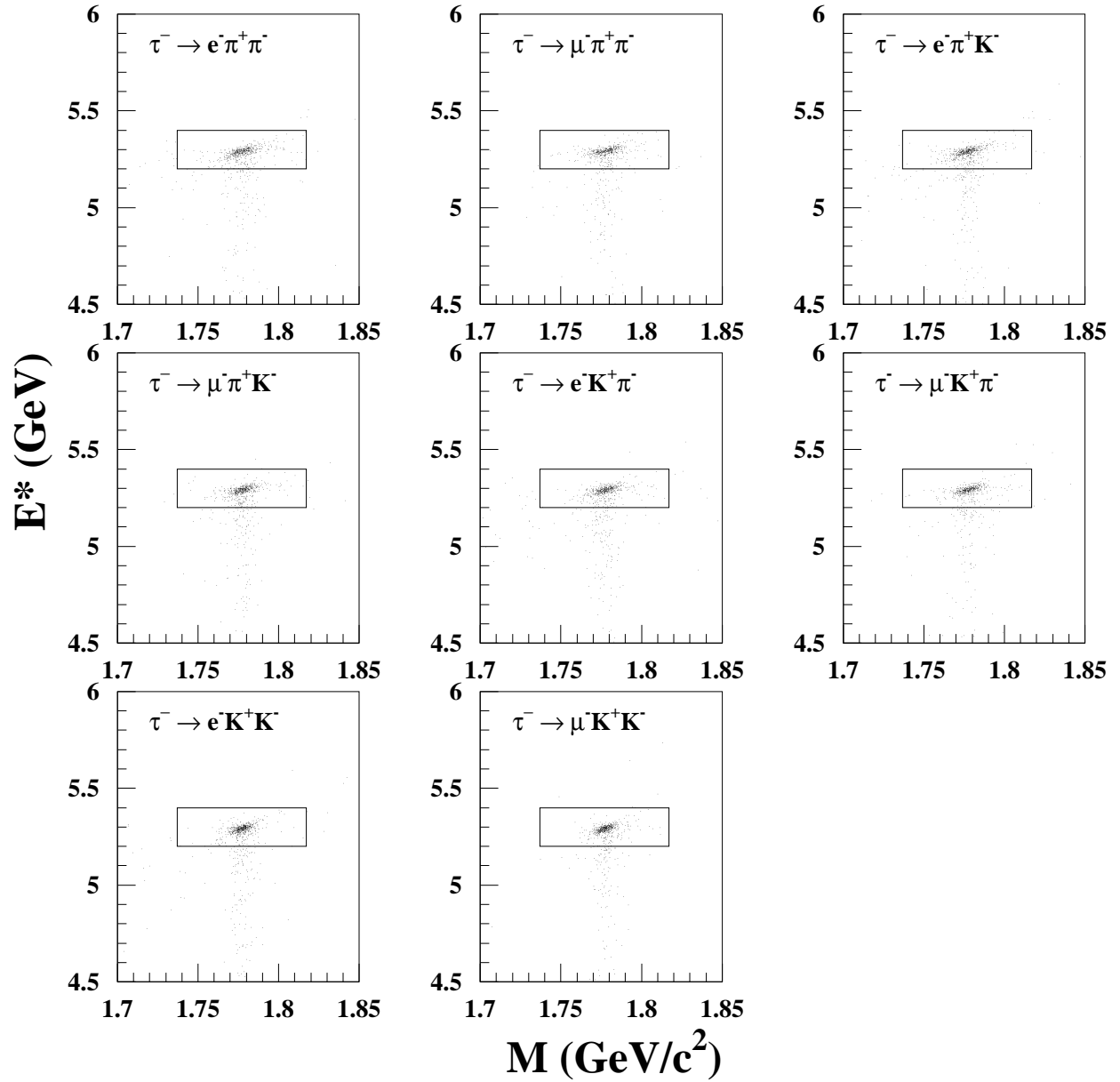Figure A.5: E^* vs M distributions of each signal Monte Carlo.($\tau \to \ell\ell\ell$)

59

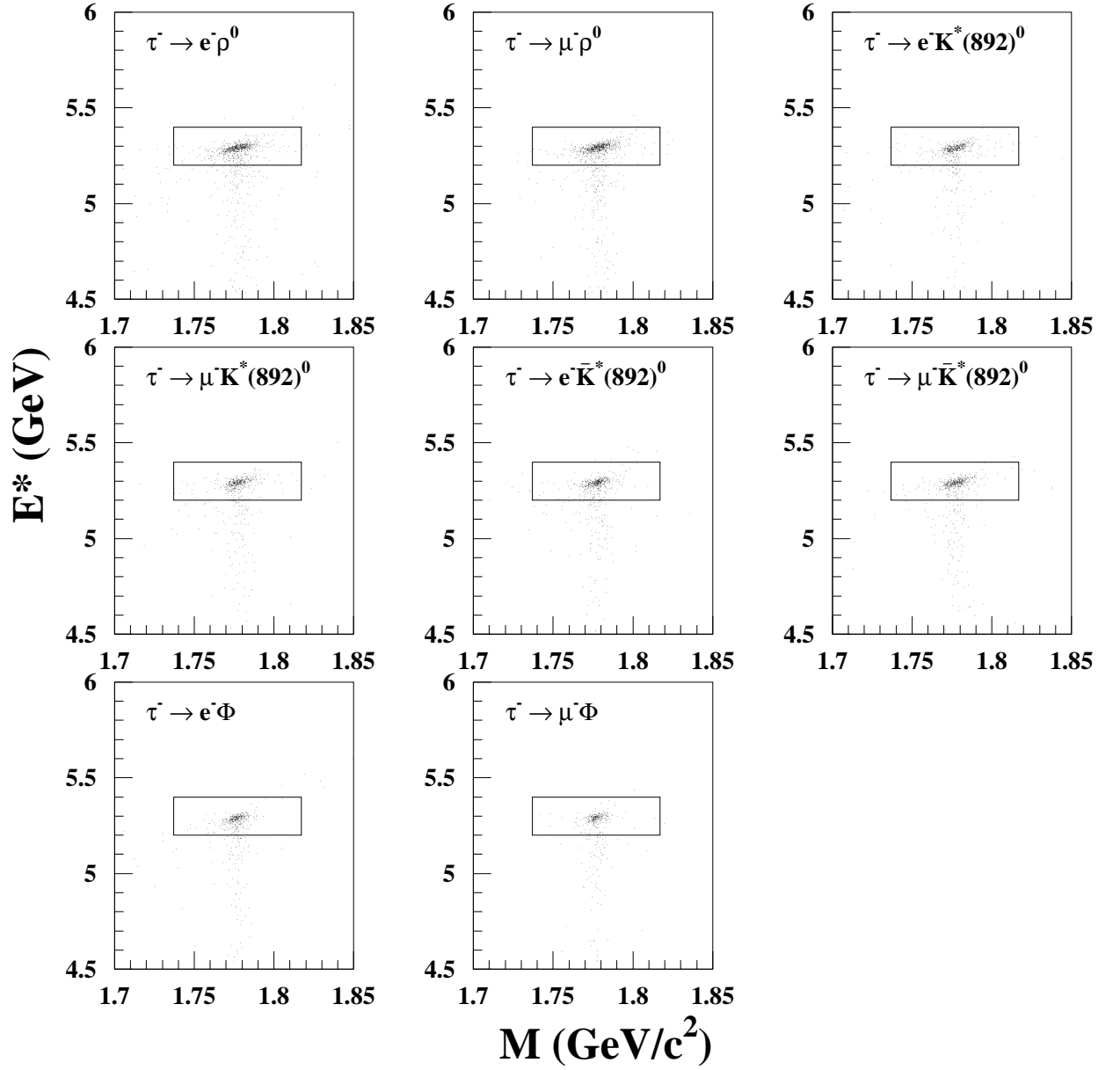Figure A.6: E^* vs M distributions of each signal Monte Carlo.($\tau \to \ell h h$)

Figure A.7: E^* vs M distributions of each signal Monte Carlo.($\tau \to \ell M^0$)

Bibliography

[1] Y. Fukuda *et al.*, Phys. Rev. Lett. **81** (1998) 1562.

[2] A. Ilakovac *et al.*, Phys. Rev. **D 52** (1995) 3993.

[3] G. Duplančić, A. Ilakovac, Proceeding of Sixth international workshop on τ lepton physics. (2000),
<http://tau2000.phys.uvic.ca/presentations/ilakovac_tau2k.ps>

[4] KEKB B Factory Design Report, KEK Report 95-7 (1995), unpublished; Y. Funakoshi *et al.*, Proc.2000 European Particle Accelerator Conference, Vienna (2000).

[5] K.G. Hayes *et al.*, Phys. Rev. **D 25** (1982) 1982.

[6] D.W. Bliss *et al.*, Phys. Rev. **D 57** (1998) 5903.

[7] Belle Collaboration, A. Abashian *et al.*, PRL **86** (2001) 2509.

[8] BABAR Collaboration, B. Aubert *et al.*, PRL **86** (2001) 2515.

[9] J. Bernabéu, A. Santamaria, J. Vidal and J.W.F. Valle, Phys. Lett. **B 187** (1987) 303.

[10] Zralek *et al.*, hep-ph/9910279.

[11] Belle Collaboration, K. Abe *et al.*, KEK Progress Report **2000-4** (2000), to be published in Nucl. Inst. and Meth. A.

[12] G. Alimonti *et al.*, Nucl. Instrum. Methods **A 453**, 71 (2000). Belle SVD Group, "Technical Design Report of Belle SVD" (1998).

[13] H. Hirano *et al.*, Nucl. Instrum. Methods **A 455**, 294 (2000); M. Akatsu *et al.*, Nucl. Instrum. Methods **A 454**, 322 (2000).

[14] T. Iijima *et al.*, Nucl. Instrum. Methods **A 453**, 321 (2000).

[15] TH. Kichimi *et al.*, Nucl. Instrum. Methods **A 453**, 315 (2000).

[16] H. Ikeda *et al.*, Nucl. Instrum. Methods **A 441**, 401 (2000).

[17] A. Abashian *et al.*, Nucl. Instrum. Methods **A 449**, 112 (2000).

[18] Belle Collaboration, "Belle progress report 1995 April - 1996 March", KEK Progress Report 96-1 (1996).

[19] R. Brun *et al.*, GEANT 3.21, CERN Report No. DD/EE/84-1 (1987).

[20] J. Jadach and Z. Was, Comp. Phys. Commun. **85** (1995) 453.

[21] CLEO software document homepage :
<http://www.lns.cornell.edu/public/CLEO/soft/QQ/index.html> (1998)

[22] Belle aafhb document homepage :
<http://bsunsrv1.kek.jp/secured/tautp/aafhb_readme.html> (1999)

[23] Review of Particle Physics, D.E. Groom *et al.*, Eur. Phys. J. **C 15** (2000) 1.

[24] K. Hanagaki *et al.*, "Electron Identification in Belle" (2001), to be published in NIM.

[25] A. Abashian *et al.*, "Muon Identification in the Belle Experiment at KEKB" (2001), to be published in NIM.

[26] Tracking Group in Belle, BELLE Note 327 (2000).

[27] G.J. Feldman and R.D. Cousins, Phys. Rev. **D 57** (1998) 3873; Review of Particle Physics, D.E. Groom *et al.*, Eur. Phys. J. **C 15** (2000) 1.

[28] Kid group in Belle, BELLE Note 321 (2000).